


Long-Time Equilibration Can Determine Transient Thermality

Karen V. Hovhannisyanyan^{1,*}, Somayyeh Nemati¹, Carsten Henkel¹, and Janet Anders^{1,2,†}

¹University of Potsdam, Institute of Physics and Astronomy, Karl-Liebknecht-Str. 24-25, Potsdam 14476, Germany

²Department of Physics and Astronomy, University of Exeter, Stocker Road, Exeter EX4 4QL, United Kingdom

 (Received 6 December 2022; revised 24 April 2023; accepted 16 June 2023; published 14 August 2023)

When two initially thermal many-body systems start to interact strongly, their transient states quickly become non-Gibbsian, even if the systems eventually equilibrate. To see beyond this apparent lack of structure during the transient regime, we use a refined notion of thermality, which we call g-local. A system is g-locally thermal if the states of all its small subsystems are marginals of global thermal states. We numerically demonstrate for two harmonic lattices that whenever the total system equilibrates in the long run, each lattice remains g-locally thermal at all times, including the transient regime. This is true even when the lattices have long-range interactions within them. In all cases, we find that the equilibrium is described by the generalized Gibbs ensemble, with three-dimensional lattices requiring special treatment due to their extended set of conserved charges. We compare our findings with the well-known two-temperature model. While its standard form is not valid beyond weak coupling, we show that at strong coupling it can be partially salvaged by adopting the concept of a g-local temperature.

DOI: [10.1103/PRXQuantum.4.030321](https://doi.org/10.1103/PRXQuantum.4.030321)

I. INTRODUCTION

Equilibration and thermalization in closed quantum many-body systems have received a lot of attention over the past two decades, leading to tremendous successes in understanding the conditions under which equilibration happens [1–4] and the properties of the (sometimes thermal) equilibrium itself [1,3,5–8]. However, only two general “expected behaviors” are known about the *transient* regime [9]. First, for a small subsystem weakly coupled to the rest of the large system, one expects Markovianity of the dynamics [10–12]. Second, when two well-separated relaxation time scales are present, some observables will typically show prethermalization [4,13–16]. In this work, we propose a qualitatively new transient behavior for a generic physical setting and then provide numerical evidence demonstrating that it indeed occurs in harmonic lattices.

The setting we consider—generic in mesoscopic and macroscopic physics—is that of two large quantum many-body systems, $X = A$ and $X = B$, of comparable size. Initially, they do not interact and start uncorrelated, each

in a *global* Gibbs state,

$$\tau(T_X, H_X) := \frac{1}{Z_X} e^{-H_X/T_X}. \quad (1)$$

Here, H_X is the Hamiltonian of X and T_X is a temperature in units $k_B = 1$, with $Z_X := \text{Tr}[e^{-H_X/T_X}]$ being the partition function. Because this (standard) definition focuses on each whole many-body system, we call it *global thermality*.

Then, in a sudden quench, coupling between the two systems is switched on, as depicted in Fig. 1. The total system state $\rho_{AB}(t)$ then evolves under the unitary evolution generated by the postquench constant total Hamiltonian $H_{\text{tot}} := H_A \otimes \mathbb{I}_B + \mathbb{I}_A \otimes H_B + H_{\text{int}}$, where H_{int} is the interaction term and \mathbb{I}_X is the identity operator on the Hilbert space of X .

The textbook expectation for weakly coupled macroscopic systems A and B is that the evolution progresses quasistatically and thus each of them retains global thermality [see Eq. (1)] at all times t , while gradual heat exchange brings the systems to a shared thermal equilibrium [17]. In other words, the individual states of A and B obey $\rho_X(t) \approx \tau(T_X(t), H_X)$, with evolving temperatures $T_X(t)$ such that $T_A(t), T_B(t) \rightarrow T^{\text{eq}}$. When the coupling is such that thermal gradients arise within X , the expectation is still that each small, localized portion of X maintains a Gibbs state with respect to its local Hamiltonian [17–20], at all times. Down to the mesoscopic scale, the assumption of instantaneous (local) thermality is the cornerstone of the two-temperature model (TTM) in solid-state physics

*karen.hovhannisyanyan@uni-potsdam.de

†janet@qipc.org

Published by the American Physical Society under the terms of the [Creative Commons Attribution 4.0 International](https://creativecommons.org/licenses/by/4.0/) license. Further distribution of this work must maintain attribution to the author(s) and the published article’s title, journal citation, and DOI.

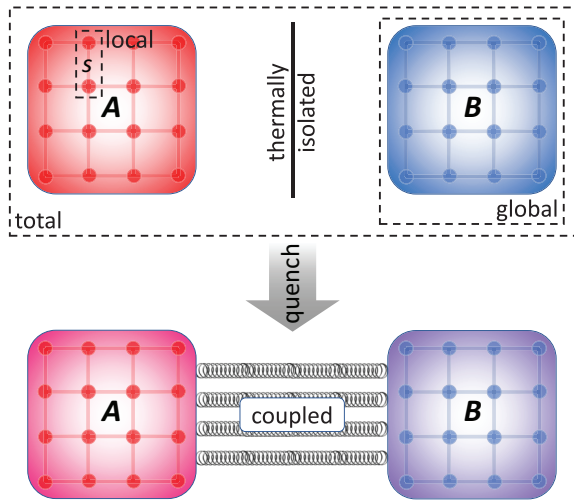


FIG. 1. The general setup. Two quantum many-body systems, $X = A$ and $X = B$, start noninteracting and uncorrelated, each in a (global) Gibbs state given by Eq. (1). Then, in a sudden quench, interaction between them is switched on. As a result, neither A nor B will generally maintain global thermality during the joint postquench unitary evolution. Here, we establish in what sense a more local notion of thermality may be maintained during the evolution. The dashed boxes illustrate our scale terminology: “total” refers to AB -wide, “global” to either A or B , and “local” pertains to small subsystems s within A or B .

[21–24]. It is designed to describe the joint dynamics of electrons and phonons in a solid after the electrons are suddenly heated up by radiation. Due to its simplicity, the TTM has been extensively employed for fitting the results of experiments and *ab initio* calculations [23–30].

However, when the coupling between and within the two global systems is not weak, then neither the assumption of global thermality nor that of local thermality of each A and B is valid any longer [31–34]. Taking this general observation as a starting point, in this paper we ask whether, and in what sense, these many-body systems may nevertheless keep appearing globally thermal when observed locally, i.e., on small subsystems.

To answer this, we begin by stating a new framework of thinking about thermality in Sec. II, which subsumes the standard definition of thermality, given in Eq. (1). It relies on both global and local properties of the system and hence defines a new concept of thermality that we call “g-local.” Its efficacy is demonstrated on harmonic lattices, a realistic yet efficiently simulable system [10,11,17,35,36], which we introduce in Sec. III. By numerically solving their dynamics, we establish in Sec. IV how well g-local thermality captures the instantaneous states of the coevolving systems. In Sec. V, we look at the process of equilibration and discuss the subtleties of constructing the generalized Gibbs ensemble (GGE) that describes it. We close with a brief discussion of implications for the validity of the TTM ansatz in Sec. VI, before concluding in Sec. VII.

Our main result is that *if* local observables of the total system AB equilibrate for long times, then A and B each maintain g-local thermality to a very good approximation at all times, including the transient regime. Moreover, this behavior is valid at all coupling strengths, including very strong coupling. This all-time validity of g-local thermality is surprising because, in general, the dynamics during the transient regime is thought to be structureless. The result thus fleshes out a novel “expected behavior” for the process of joint equilibration of two large systems.

II. G-LOCAL THERMALITY

Consider a state ρ_X of a many-body system X and a small local subsystem $s \subset X$ (see Fig. 1). We ask whether a temperature T exists such that the reduced state $\rho_s = \text{Tr}_{X \setminus s}[\rho_X]$ of s obeys

$$\rho_s \stackrel{?}{=} \text{Tr}_{X \setminus s}[\tau(T, H_X)], \quad (2)$$

where the partial trace is taken over all of X except s . If this condition is obeyed, then we say that X is “g-locally thermal at s .” The term “g-local” is to emphasize that while ρ_s is a *local* quantity, it contains information about the *global* $\tau(T, H_X)$ due to non-negligible interactions within X . Furthermore, if X is g-locally thermal at each small subsystem, then we call X “g-locally thermal.” If, in addition, T is the same for all of them, then we call X “uniformly g-locally thermal.” Otherwise, when T varies depending on the subsystem, we say that X is “g-locally thermal with a gradient.”

Note that the condition given in Eq. (2) is not to be confused with subsystem s being in a Gibbs state $\tau(T, H_s)$ at T with respect to its local (bare) Hamiltonian H_s . Indeed, it is well known that ρ_s can differ significantly from $\tau(T, H_s)$ [8,31–33,37–42]. Instead, partially reduced states of global Gibbs states,

$$\tau_s^{\text{MF}}(T) := \text{Tr}_{X \setminus s}[\tau(T, H_X)], \quad (3)$$

are known as “mean-force (Gibbs) states” [7,43–45]. With this definition, the condition of “g-local thermality of X ” can be compactly expressed as

$$\rho_s \stackrel{!}{=} \tau_s^{\text{MF}}(T), \quad \forall s \subset X, \quad (4)$$

where the s are small subsystems.

However, in most realistic scenarios, one cannot expect the equality in Eq. (4) to be exact. Thus, it is sensible to introduce an effective g-local temperature T_s^{eff} for each subsystem $s \subset X$ as that of the mean force state $\tau_s^{\text{MF}}(T)$ that is closest to ρ_s . Namely,

$$T_s^{\text{eff}} := \arg \min_T \mathcal{D}[\rho_s, \tau_s^{\text{MF}}(T)], \quad (5)$$

where as a measure of distance \mathcal{D} between the two states, we choose the Bures metric [46] (for the definition, see

Appendix A). The distance

$$\mathcal{D}_s^{\min} := \min_T \mathcal{D}[\rho_s, \tau_s^{\text{MF}}(T)] \quad (6)$$

then measures the extent to which ρ_s deviates from the optimal mean-force Gibbs state. In what follows, we use the dual quantity, the *fidelity* [46],

$$\mathcal{F}_s^{\max} := [1 - (\mathcal{D}_s^{\min})^2/2]^2 \leq 1, \quad (7)$$

and we call this the degree of g-local thermality of X at s . The fidelity is 1 if and only if the two states ρ_s and τ_s^{MF} are equal, in which case T_s^{eff} turns into a proper g-local temperature for s . Therefore, the higher the \mathcal{F}_s , the closer the local system s is to having a well-defined g-local temperature [see Eq. (5)].

The pair $(T_s^{\text{eff}}, \mathcal{F}_s^{\max})$ thus fully characterizes the g-local thermality of X at subsystem s . If the T_s^{eff} for essentially all small $s \subset X$ are approximately equal to each other and all \mathcal{F}_s^{\max} 's are close to 1 (within a chosen error [47]), then ρ_X (or X itself) is g-locally thermal, with uniform temperature T_X^{eff} . In Sec. IV, we use T_s^{eff} and \mathcal{F}_s^{\max} to assess the g-local thermality of each of the two global systems, A and B , of comparable size N , during their joint evolution.

Unmistakably, our framework is inspired by the equivalence of ensembles [48–52] and canonical typicality [3, 53, 54]. The difference is in how temperature is defined. There, the effective temperature $T_X^{\text{eff,can}}$ is determined by equating the mean energies, i.e.,

$$\text{Tr}[\tau(T_X^{\text{eff,can}}, H_X)H_X] = \text{Tr}[\rho_X H_X], \quad (8)$$

and it is shown that Eq. (2) is satisfied for $T = T_X^{\text{eff,can}}$ under certain conditions on H_X and ρ_X . This approach is thus energy-centric and global: $T_X^{\text{eff,can}}$ is the same for all subsystems. In contrast, our framework is state-centric and local: it directly accesses the marginal state of a subsystem s and defines T_s^{eff} as the solution of the optimization problem in Eq. (6). The ability to define a local degree of thermality and an associated temperature at each subsystem allows our framework to accommodate systems with a temperature gradient (for an example, see Appendix D), which is beyond the reach of the typicality-based approaches. Note that when H_X is a sum of local terms and the system is g-locally thermal with a uniform g-local temperature T_X^{eff} , then the two temperatures coincide: $T_X^{\text{eff,can}} = T_X^{\text{eff}}$ (see Appendix B).

Lastly, when the size of the system X is finite, then Eq. (2) will hold for a system in a canonically typical state only approximately, with the correction going to zero as $N_s/N_X \rightarrow 0$, where N_s and N_X are the numbers of sites in s and X , respectively. Similarly, in our framework, we expect \mathcal{D}_s^{\min} to also have a positive contribution stemming from the small parameter N_s/N_X in realistic scenarios. This

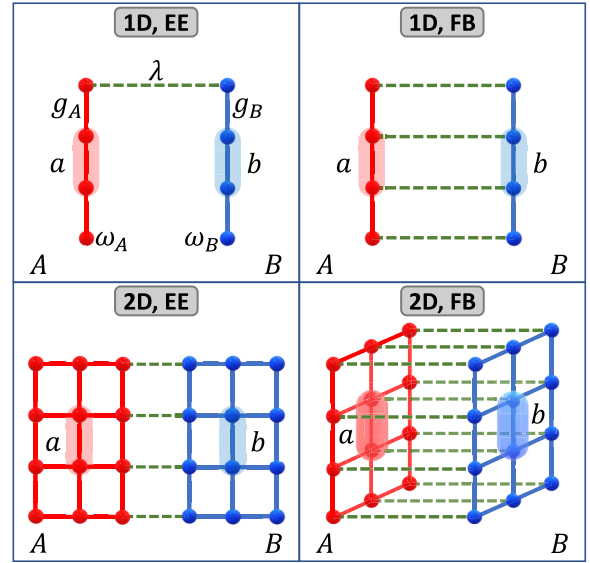


FIG. 2. A schematic of the model. Systems A (red) and B (blue) are here modeled as one-dimensional (1D) (top row) or two-dimensional (2D) (bottom row) harmonic lattices. Each site (circles) denotes a local oscillator of frequency ω_X that is coupled to its neighbors with strength g_X (solid lines) [cf. Eq. (9)]. While only nearest-neighbor interactions are depicted, our results apply also to long-range interacting systems. Intersystem coupling (dashed green lines) with strength λ occurs either only at the system edges—as shown in the left column [edge–edge (EE) coupling], or at all sites—as shown on the right column [full-body (FB) coupling] [see Eq. (11)]. In all panels, example subsystems a and b are depicted, at which the g-local thermality of each, A and B , is assessed in Sec. IV.

finite-size contribution will likely be a highly complex function of N_s/N_X [54, 55] and the line between “small” and “big” subsystems will be drawn by this system- and situation-dependent contribution and one’s error tolerance. Importantly, the finite-size effect will in general not be the only factor contributing to \mathcal{D}_s^{\min} .

III. SETUP AND MODEL

As mentioned in Sec. I, our setup consists of two large many-body systems, A and B , coevolving after an interaction between them is switched on. To be able to solve the dynamics of the total system AB and demonstrate the occurrence (or absence) of g-local thermality of each, A and B , we choose harmonic lattices. Despite their simplicity, these systems are routinely used to approximate various physical systems [10, 11, 17, 35, 36]. At the same time, the dynamics of the Gaussian states in these systems admit a numerically efficient phase-space representation [56–58], allowing us to directly simulate few-hundred-particle lattices.

Each global system is a one-dimensional (1D) or two-dimensional (2D) translation-invariant open-ended lattice

(see Fig. 2), with Hamiltonian

$$H_X = \sum_{\nu} \left[\frac{\omega_X^2 q_{X,\nu}^2}{2} + \frac{p_{X,\nu}^2}{2} \right] + \sum_{\nu,\nu'} G_X^{\nu,\nu'} q_{X,\nu} q_{X,\nu'}, \quad (9)$$

where ν enumerates the sites in lattice X , ω_X is the on-site frequency of each site, and all masses are set to 1. The intrasystem coupling function, $G_X^{\nu,\nu'}$, depends only on the distance between the sites ν and ν' . Our numerical samples below explore lattices with coupling functions of the form

$$G_X^{\nu,\nu'} = \frac{g_X}{\text{dist}(\nu, \nu')^\alpha}, \quad (10)$$

where $\text{dist}(\nu, \nu')$ is the Manhattan distance between the sites ν and ν' and $\alpha > 0$ quantifies the *range* of interactions. Nearest-neighbor interactions correspond to $\alpha = \infty$ (and couple only sites with $\text{dist}(\nu, \nu') = 1$).

We recall that A and B are large and of comparable size. Therefore, for simplicity of presentation, we choose the lattices A and B to have the same size and shape, with $N \gg 1$ denoting the number of sites in each of them. The opposite limit, where one of the systems is much smaller than the other—say, $N_A \ll N_B$ —is well understood in harmonic systems. A then simply thermalizes with B , in the sense that its state tends to $\text{Tr}_B[\tau(T_B, H_{AB})]$ (save for finite-size effects) [59,60].

For the interaction term between A and B , H_{int} , we consider two types of coupling: edge–edge (EE) and full-body (FB), shown in Fig. 2 for 1D and 2D lattices. For example, the FB interaction has the form

$$H_{\text{int}}^{(\text{FB})} = \lambda \sum_{\nu} q_{A,\nu} q_{B,\nu}, \quad (11)$$

where λ is the intersystem coupling strength and ν runs over *all* corresponding sites in A and B (see the right column of Fig. 2). Given the form of Eqs. (9) and (11), the natural dimensionless coupling constants are g_X/ω_X^2 and $\lambda/(\omega_A\omega_B)$.

For the initial state, we take the uncorrelated state

$$\rho_{AB}(0) = \tau(T_A, H_A) \otimes \tau(T_B, H_B) \quad (12)$$

and the evolution of the joint system AB is generated by the total Hamiltonian H_{tot} . The Gaussian theory that underpins the simulation of harmonic systems has been reviewed in, e.g., Refs. [56–58]. We give a brief account of the main quantities and formulas used in our simulations in Appendix C. Using these methods, we numerically solve the dynamics of [1D,EE], [1D,FB], [2D,EE], and [2D,FB] lattices for a representative selection of the full range of parameter values for which the spectrum of H_{tot} is bounded from below [61].

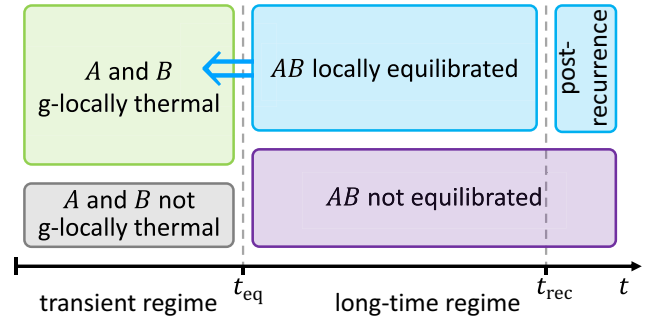


FIG. 3. An illustration of the main result. Our main result is that *if* local equilibration occurs at long times, i.e., $\rho_s(t) \approx \rho_s^{\text{eq}}$ for all small subsystems $s \subset AB$ for $t \in [t_{\text{eq}}, t_{\text{rec}}]$ (see Sec. V), *then* A and B are g-locally thermal at any time t , also in the transient regime (see Sec. IV). Namely, $\rho_s(t) \approx \tau_s^{\text{MF}}(T_s^{\text{eff}}(t))$, where $T_s^{\text{eff}}(t)$ is a time-dependent g-local temperature of subsystem s (see Sec. II). Remarkably, this result characterizes the transient regime and links it with the long-time equilibration behavior of the system.

Our direct simulation of the dynamics of the total system AB gives us access to $\rho_A(t)$ and $\rho_B(t)$, which allows us to analyze the g-local thermality of A and B at all times during their joint postquench evolution.

IV. ALL-TIME G-LOCAL THERMALITY

We have performed a large number of numerical experiments spanning the full parameter range and established the following. G-local thermality of A and B is guaranteed *at all times, including transient times*, whenever *all local observables of AB equilibrate dynamically at long times* (for further details on this requirement, see Sec. V). This behavior occurs for all intralattice coupling strengths g_X and interaction ranges α and interlattice couplings λ . This is the first main result of the paper. An illustration of this relation between long-time and transient behavior is shown in Fig. 3. A detailed account on how we perform the numerical proof, as well as the numerical evidence itself, can be found in Appendix E.

An immediate practical consequence of this result is that if an experimenter monitoring a small region of the system notes that g-local thermality is violated at that location, then they can predict with certainty that the system will *not* ever equilibrate as a whole.

An example illustration of the above general result is given by Fig. 4. It shows the fidelities and effective temperatures for the case where A and B are both open-end 1D chains of 200 sites with long-range interactions within them ($\alpha = 0.5$), which are coupled via a full-body (FB) interaction Hamiltonian (see Fig. 2). The plots in Fig. 4 are for subsystem a consisting of two consecutive sites in the middle of chain A and, similarly, for b in B . Figure 4(a) shows the degree of g-local thermality of A at a (red) and of

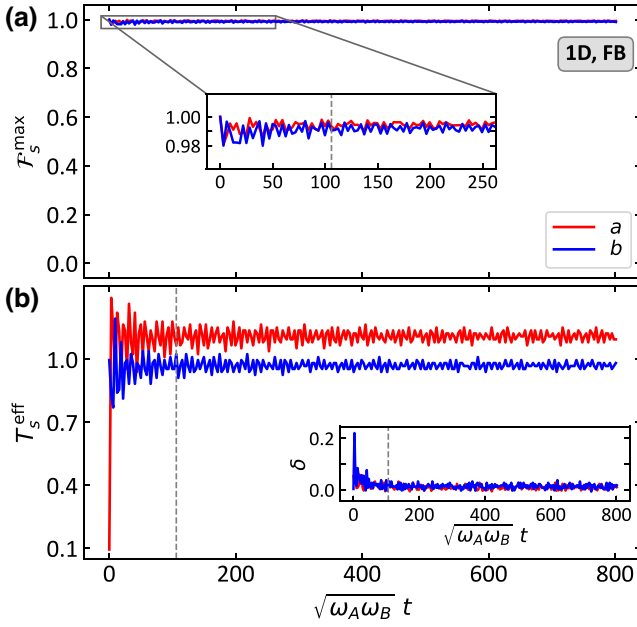


FIG. 4. The g-local thermality of A at a and B at b . (a) The fidelity \mathcal{F}_s^{\max} [see Eq. (7)], which measures the degree of g-local thermality of A at $s = a$ (red) and of B at $s = b$ (blue), as a function of time t . The inset zooms into the fidelity at early times. (b) The corresponding effective g-local temperatures T_s^{eff} defined in Eq. (5). The inset shows the normalized difference $\delta = (T_X^{\text{eff,can}} - T_X^{\text{eff}})/T_X^{\text{eff}}$ between the g-local and effective canonical [see Eq. (8)] temperatures. The fidelities are close to 1, indicating that both A and B are g-locally thermal at a and b , respectively, with very good precision at all times during the evolution. Note that subsystems a and b settle to slightly different g-local temperatures. This plot is for a and b each consisting of two consecutive sites situated at the centers of the 1D chains A and B , respectively. The chains are $N_A = N_B = 200$ long and interact through full-body (FB) coupling. Each chain features long-range interactions, with the decay rate $\alpha = 1/2$ [cf. Eq. (10)]. The rest of the Hamiltonian parameters are $\omega_A = 2$ and $g_A/\omega_A^2 = 0.2$ for A and $\omega_B = 1.5$ and $g_B/\omega_B^2 = 0.3$ for B , and the interchain coupling is $\lambda/(\omega_A \omega_B) = 0.5$. The initial temperatures are $T_A = 0.1$ and $T_B = 1$. The vertical dashed lines in both panels (a) and (b) indicate the instance at which Fig. 6 is plotted.

B at b (blue), as defined in Eq. (7). As we can see, they are close to 1 at all times, demonstrating the g-local thermality of A at a and B at b . The corresponding time-evolving effective g-local temperatures T_a^{eff} and T_b^{eff} of the small subsystems a (red) and b (blue) are shown in Fig. 4(b). These g-local temperatures slowly converge in time, while oscillating about each other. The apparent symmetric nature of these oscillations is due to the fact that the interaction energy remains small for the chosen set of parameters (see Sec. VI with Fig. 10 and the discussion in Appendix B).

To appreciate the nontriviality of the high values of the fidelity in Fig. 4, note that $\lambda = 0.5 \omega_A \omega_B$ corresponds to quite strong coupling. Indeed, it is close to the maximal coupling strength ($\lambda_{\max} \approx 0.695 \omega_A \omega_B$), consistent with

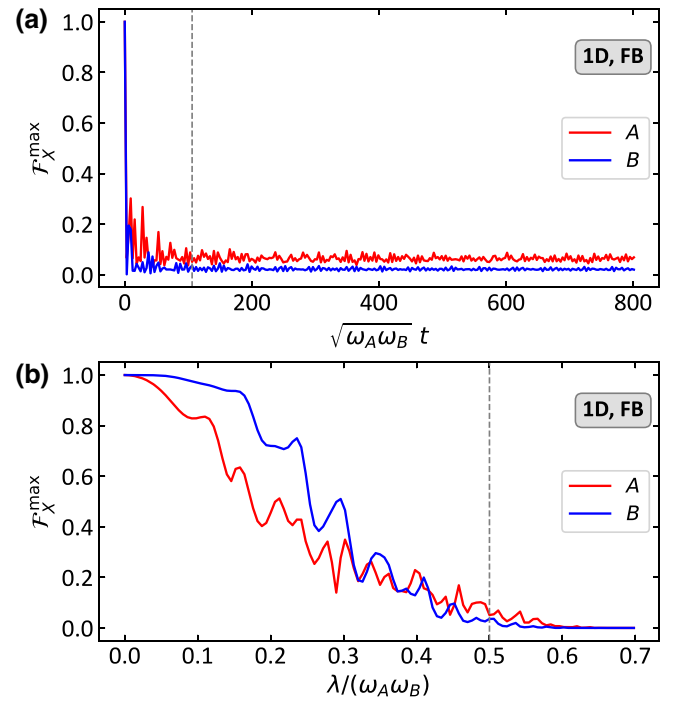


FIG. 5. The global non-Gibbsianity of A and B . (a) The fidelity \mathcal{F}_X^{\max} of the state $\rho_X(t)$ of many-body system $X = A, B$ with the closest global Gibbs state [see Eq. (1)] as a function of time t . Starting from a global Gibbs state for which the fidelity is 1, the state of X deviates increasingly from Gibbs form with an increasing interaction time between A and B . The interchain coupling for this panel is $\lambda/(\omega_A \omega_B) = 0.5$, as in Fig. 4. (b) The fidelity \mathcal{F}_X^{\max} of the state $\rho_X(t_0)$ at a fixed moment of time t_0 as a function of the coupling strength λ , for $\lambda \in [0, \lambda_{\max}]$, where $\lambda_{\max} \approx 0.695 \omega_A \omega_B$ is the largest value allowed for $|\lambda|$ in this configuration. The time $\sqrt{\omega_A \omega_B} t_0 = 106$ [the vertical dashed line in (a)] is chosen so as to allow AB to evolve considerably away from its initial state. The dashed line shows the coupling strength at which (a) is plotted. Both panels (a) and (b) are for the same [1D, FB] configuration, with all other parameters being the same as in Fig. 4.

the requirement that H_{tot} must be bounded from below, with all the other parameters fixed. Moreover, $\lambda/g_A = 1.875$ and $\lambda/g_B \approx 2.222$, which means that the coupling strongly perturbs all the nodes of both A and B . Nonetheless, both A and B maintain a high degree of g-local thermality (≥ 0.98) at all times. For comparison, for the not-much-larger $\lambda = 0.65 \omega_A \omega_B$, \mathcal{F}_a^{\max} and \mathcal{F}_b^{\max} get as low as 0.93 and 0.884, respectively, during the evolution.

Moreover, the all-time high degree of g-local thermality of A and B in Fig. 4 is in stark contrast to the quick loss of global thermality by them, especially at higher coupling strengths. Similarly to Eqs. (6) and (7), we quantify the degree of global thermality of system X as $\mathcal{F}_X^{\max}(t) := \max_T \mathcal{F}[\rho_X(t), \tau(T, H_X)]$. Figure 5 shows the result for the same [1D, FB] system as in Fig. 4. We see that the degree of global thermality in Fig. 5 quickly drops from 1 to

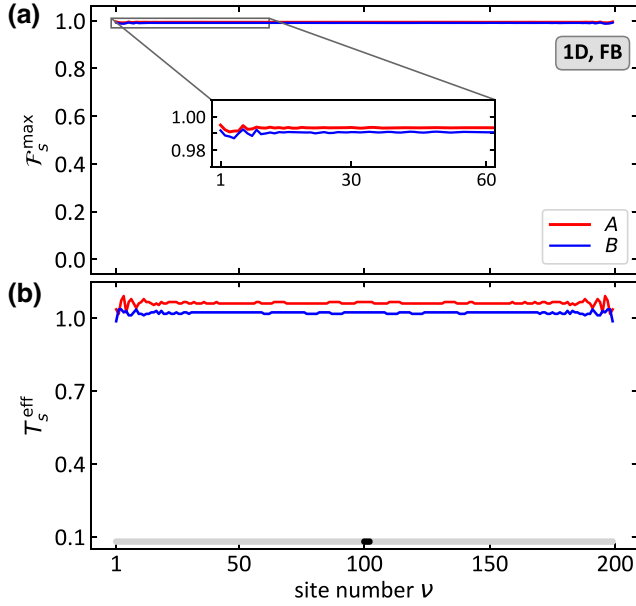


FIG. 6. The g-local thermality with site number ν . (a) The degree of g-local thermality \mathcal{F}_s^{\max} [see Eq. (7)] of A at two-site subsystem $s = a$ (red) and of B at $s = b$ (blue), respectively. (b) The corresponding effective temperatures T_s^{eff} [see Eq. (5)] as a function of the site number ν . Here, $\nu = 1, \dots, N - 1$ labels *all* subsystems consisting of two neighboring sites in A and B . The fidelities are very close to 1 for all ν . Furthermore, all subsystems s located away from the edges, i.e., those “inside the bulk,” give essentially the same g-local temperature T_s^{eff} . Together, these two plots show that both A and B are uniformly g-locally thermal at *all* two-site subsystems. The “slider” (black dot) at the bottom indicates the position of subsystem s in X at which Fig. 4 is plotted. We highlight that this is just one representative snapshot of the g-local properties of A and B at any particular moment in time; here, $\sqrt{\omega_A \omega_B} t_0 = 106$. We observe qualitatively the same plots for *any small subsystem size* (see Fig. 7) and at other time points (with varying temperatures; see Fig. 4). All other parameters are as in Figs. 5 and 4.

$\lesssim 0.05$, which is a clear indication that the global state is not Gibbsian [62].

Lastly, we find that for most parameter choices for which the total system AB *does not* locally equilibrate at long times (purple box in Fig. 3), the global systems A and B do not develop stable g-local thermality. However, there do exist parameter values for which AB does not equilibrate but A and B do still maintain g-local thermality at all times.

Now moving on from the specific two-site subsystems located in the respective centers of the chains, the plots in Fig. 6 show that 1D chains A and B are g-locally thermal with respect to *all* two-site subsystems ν along the chains. Moreover, “inside the bulk,” i.e., away from the edges inward, all two-site subsystems share the same temperature. Both A and B are thus uniformly g-locally thermal.

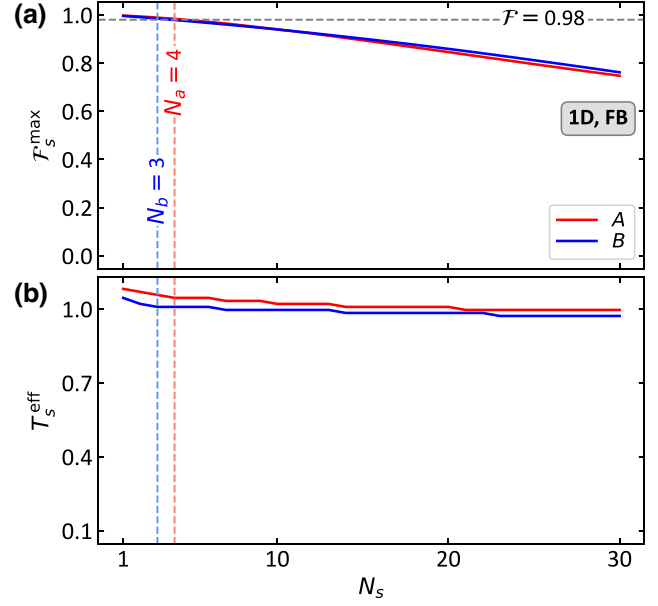


FIG. 7. The g-local thermality with subsystem size N_s . (a) The degree of g-local thermality [see Eq. (7)] of X at an N_s -site subsystem s for $N_s = 1, 2, \dots$. All subsystems s are centered within X and all the other parameters are as in Figs. 5–6. The plot is taken at the instance $\sqrt{\omega_A \omega_B} t_0 = 106$. \mathcal{F}_s^{\max} is high (≥ 0.98) up to subsystem sizes $N_a = 4$ and $N_b = 3$ for these 1D chains of $N_A = N_B = 200$. (b) The effective g-local temperatures T_s^{eff} [see Eq. (5)] versus N_s . These values can be considered trustworthy only up to $N_a = 4$ and $N_b = 3$, respectively. Interestingly, we find that they do not change significantly as the subsystem size goes beyond $N_s = 4$.

Of course, as the size of the subsystem s grows, the degree to which the system X is g-locally thermal at s , \mathcal{F}_s^{\max} , must decrease, reaching very low values as N_s approaches N_X (see Fig. 5, which plots the fidelity for $N_s = N_X$). The decrease of \mathcal{F}_s^{\max} with N_s is shown in Fig. 7, where the center of subsystem s is fixed at the center of X . The plot is a snapshot of the system taken at the same instance $\sqrt{\omega_A \omega_B} t_0 \approx 106$ as in Fig. 6. The presented behavior is representative for all times. We see that $\mathcal{F}_s^{\max} \geq 0.98$ for $N_a \leq 4$ and $N_b \leq 3$. The effective g-local temperatures T_s^{eff} for all values of N_s are approximately equal. For larger values of time as well as for larger sizes of the global systems, both curves in Fig. 7 become flatter. However, they do not become entirely flat in the $N_X \rightarrow \infty$ limit for all times. Thus, although A and B are indeed g-locally thermal to a good approximation at all times for $N_X \gg 1$, Eq. (4) does not become *exact* in the thermodynamic limit (at least not for all times).

The g-local thermality that we observe is not limited to the [1D, FB] case. We find qualitatively identical behavior for the other three topological configurations [1D, EE], [2D, EE], and [2D, FB] (see Fig. 1). To provide representative evidence, in Fig. 8 we show the time dependence

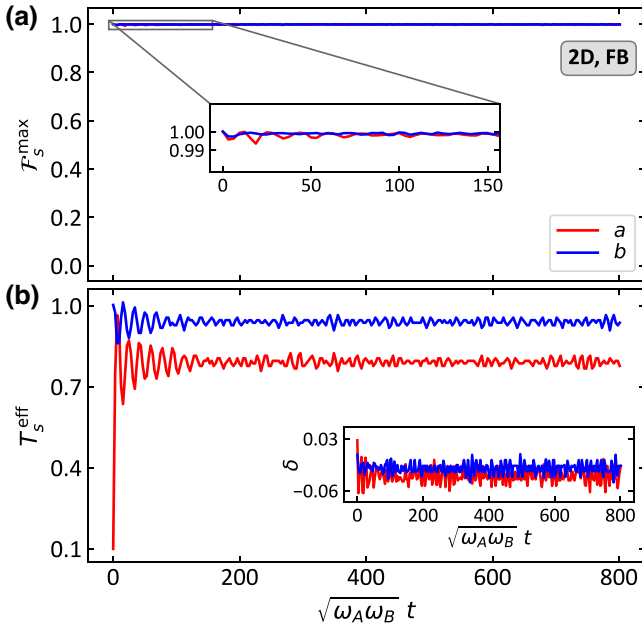


FIG. 8. The g-local thermality for [2D, FB]. The analogue of Fig. 4 for a [2D, FB] system (bottom-right corner of Fig. 2). A and B are 26×26 2D lattices, with nearest-neighbor coupling within them [$\alpha = \infty$ in Eq. (10)] and full-body coupling between them. The subsystems a and b are two-site subsystems located centrally in A and B , respectively. On panel (a), we observe very high degrees of g-local thermality in both A and B for all times. Moreover, on panel (b), we see a faster temperature stabilization than in Fig. 4(b). The inset shows the relative temperature difference δ between T_X^{eff} and $T_X^{\text{eff,can}}$. Similarly to the 1D case, the subsystems a and b settle to slightly different g-local temperatures. Here, the Hamiltonian parameters are $\omega_A = 2$ and $g_A/\omega_A^2 = 0.15$ for A and $\omega_B = 1.5$ and $g_B/\omega_B^2 = 0.2$ for B and the interchain coupling is $\lambda/(\omega_A\omega_B) = 0.23$. The initial temperatures are $T_A = 0.1$ and $T_B = 1$.

of the fidelities and effective g-local temperatures for central two-site subsystems a and b for the [2D, FB] case. There, A and B are 2D lattices of dimension 26×26 (i.e., $N = 676$) with full-body interaction. These [2D, FB] plots show qualitative similarity to those for the [1D, FB] case, shown in Fig. 4, with slightly better convergence compared to the 1D case. Both Figs. 4 and 8 illustrate the important possibility of the g-local temperatures of A and B not converging to the same value (cf. Sec. VI). This behavior can occur both in strong- and weak-coupling regimes.

For the [1D, EE] and [2D, EE] configurations, we find that, while both A and B remain g-locally thermal, the systems expectedly exhibit gradients of local temperatures. We discuss this in Appendix D.

A. Independence from typicality

Finally, the novelty and unexpectedness of our all-time g-local thermality result is emphasized by the fact that it applies to systems and situations well beyond the scope

of all known results in canonical typicality and ensemble equivalence. Indeed, the most general result in that direction is the stronger ensemble equivalence proven by Brandão and Cramer [50] for lattices with short-range interactions. There, it is shown that if $\tau(T_X^{\text{eff,can}}, H_X)$ has exponentially decaying correlations and ρ_X is not too far from $\tau(T_X^{\text{eff,can}}, H_X)$, then ρ_s approaches $\tau_s^{\text{MF}}(T_X^{\text{eff,can}})$ in the thermodynamic limit for most small subsystems s . In our language, this means that ρ_X is g-locally thermal with uniform g-local temperature $T_X^{\text{eff}} = T_X^{\text{eff,can}}$. While the conditions under which this result applies are fairly restrictive, especially when dealing with dynamical states, it implies that our result for FB-coupled nearest-neighbor lattices could be expected to some extent. And, indeed, in the bottom inset of Fig. 8, we see that the difference between T_X^{eff} and $T_X^{\text{eff,can}}$ remains fairly small at all times. However, long-range interacting systems, as well as situations with temperature gradient, are beyond the scope of Ref. [50] (and all other works on canonical typicality and ensemble equivalence known to us). Sure enough, we find a significant discrepancy between T_X^{eff} and $T_X^{\text{eff,can}}$ in Figs. 4 and 11, signaling that the results of Ref. [50] do not hold. The persistent g-local thermality that we observe, on the other hand, applies to all these systems and situations, which strongly suggests that it is a fundamentally different phenomenon from ensemble equivalence. We provide further context and a more detailed discussion in Appendix F.

V. EQUILIBRATION AND THE GENERALIZED GIBBS ENSEMBLE

Recall that all-time g-local thermality of A and B is guaranteed whenever *all local states* of AB equilibrate at long times. Here, we first discuss the details of this requirement and then describe how the equilibrium state relates to the generalized Gibbs ensemble (GGE).

The definition of “local equilibration” [3,63] of the total system AB is that the reduced state $\rho_s(t) = \text{Tr}_{AB \setminus s}[\rho_{AB}(t)]$ of each small subsystem s of AB reaches an ϵ neighborhood of some ρ_s^{eq} within some finite time $t_{\text{eq}}(\epsilon)$ and thereafter stays in it. Typically, $t_{\text{eq}}(\epsilon)$ will depend only weakly on the size of AB , as long as AB is large enough. Note though that, in general, the larger the relative size N_s/N_{AB} of s , the larger the ϵ one has to tolerate (see also the related discussion at the end of Sec. II).

On the other hand, for a finite system of size N_{AB} , there is always an upper time limit, the recurrence time t_{rec} , at which the local equilibration behavior is disrupted and information starts flowing back from $AB \setminus s$ into the subsystem s . This time scale is typically a monotonically increasing function of N_{AB} . Hence, “local equilibration” of AB refers to being in equilibrium in the full time-interval $[t_{\text{eq}}, t_{\text{rec}}]$ [64]. Numerically, we confirm local equilibration by directly calculating $\rho_s(t)$ from $t = 0$ to some large t_{max} and plotting the distance $\mathcal{D}[\rho_s(t), \rho_s^{\text{GGE}}]$ against t . When

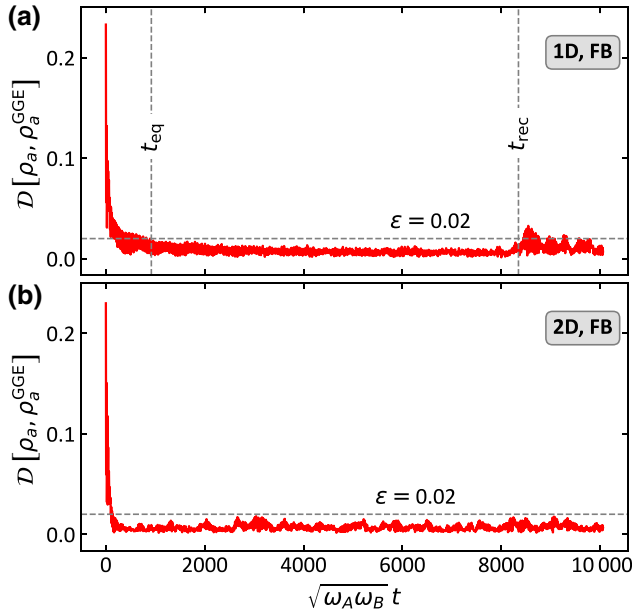


FIG. 9. Equilibration and time scales. (a) The equilibration of a two-site subsystem a in the center of A for the [1D, FB] configuration with $\alpha = 1.75$ and all the other parameters as in Fig. 8. Here, the normal-frequency spectrum is nondegenerate and therefore the equilibrium state ρ_a^{eq} equals ρ_a^{GGE} , with the latter defined in Eq. (14). Due to the finite size of AB , equilibration never occurs exactly—one usually fixes a small $\epsilon > 0$ and considers the system equilibrated once $\mathcal{D}[\rho_a(t), \rho_a^{\text{eq}}] \leq \epsilon$. We choose $\epsilon = 0.02$ here and find that s is in equilibrium for $t \in [t_{\text{eq}}, t_{\text{rec}}]$. For times larger than the “recurrence time” t_{rec} , AB deviates from local equilibrium. This t_{rec} grows with the size of AB . (b) The equilibration of a two-site subsystem at the center of A for the [2D, FB] configuration with $\alpha = 1$ and all the other parameters as in Fig. 8. The equilibrium is still described by the GGE, but one that is complemented with the additional conserved charges present in this configuration due to degeneracies in the normal-mode spectrum.

this distance goes below some small ϵ and stays there for a substantial portion of the time, then we conclude that $\rho_s^{\text{eq}} = \rho_s^{\text{GGE}}$ (for a more precise characterization, see Appendix E 2). This procedure is done for all small s .

Representative results are shown in Fig. 9 for the [1D, FB] and [2D, FB] configurations. We emphasize again that when such local equilibration of AB occurs at long times, $t > t_{\text{eq}}$, then g-local thermality of A and B holds *at all times*, including the transient time interval $[0, t_{\text{eq}}]$.

Let us now comment on the nature of the equilibrium state itself. For an integrable system (the total system AB in our case), whenever local equilibration takes place, it is generically described by the so-called generalized Gibbs ensemble (GGE) [2,3,6,14,16,65–72]. For systems with quadratic Hamiltonians (bosonic and fermionic alike), the GGE is determined only by quadratic conserved charges [68,73,74]. Whenever all the normal frequencies of the system are different from each other, the Hamiltonians of

the normal modes, which are conserved, constitute a basis in the algebra of conserved charges. Thus, when all N_{AB} normal frequencies Ω_k of the interacting harmonic lattice AB are distinct, the GGE takes the form

$$\rho_{AB}^{\text{GGE}} := \frac{e^{-\sum_{\kappa} \beta_{\kappa} h_{\kappa}}}{\text{Tr}[e^{-\sum_{\kappa} \beta_{\kappa} h_{\kappa}}]}, \quad (13)$$

where $h_{\kappa} := \Omega_{\kappa}(Q_{\kappa}^2 + P_{\kappa}^2)/2$ are the normal-mode Hamiltonians (Q_{κ} and P_{κ} being the normal-mode coordinates) of AB . By definition, the total postquench Hamiltonian can be written as $H_{\text{tot}} = \sum_{\kappa=1}^{N_{AB}} h_{\kappa}$ (see Appendix C).

The state given in Eq. (13) describes the equilibrium in the sense that [64,68]

$$t_{\text{eq}} \leq t \leq t_{\text{rec}} : \rho_s(t) \approx \text{Tr}_{AB \setminus s} [\rho_{AB}^{\text{GGE}}] := \rho_s^{\text{GGE}}, \quad (14)$$

where the approximate equality sign indicates that there will generally be a finite-size correction ϵ . In Eq. (13), $1/\beta_{\kappa}$ are the “generalized temperatures” that stem from the fact that the operators h_{κ} are conserved in the dynamics. They are determined through the initial expectation values

$$\text{Tr}[h_{\kappa} \rho_{AB}^{\text{GGE}}] = \text{Tr}[h_{\kappa} \rho_{AB}(0)], \quad \kappa = 1, \dots, N_{AB} \quad (15)$$

(for an explicit formula, see Eq. (C21)). Figure 9(a) shows local convergence to this GGE for the [1D, FB] configuration.

When the spectrum of normal frequencies has degeneracies, the operators h_{κ} no longer span the complete algebra of conserved charges [69,73,74]. More specifically, each pair $\Omega_k = \Omega_j$ ($k \neq j$) adds the conserved charge $I_{kj} = \Omega_k(Q_k Q_j + P_k P_j)$. Together with h_{κ} ’s, these now span the complete algebra of conserved charges. Therefore, in order to correctly describe the local equilibrium of the system, the GGE needs to be complemented accordingly: $\rho_{AB}^{\text{GGE}} \propto e^{-\sum \beta_{\kappa} h_{\kappa} - \sum \beta_{kj} I_{kj}}$ [69,73,74]. Similarly to Eq. (15), the β_{kj} ’s are determined from $\text{Tr}[I_{kj} \rho_{AB}^{\text{GGE}}] = \text{Tr}[I_{kj} \rho_{AB}(0)]$. Due to the presence of degeneracies, the decomposition of H_{AB} into normal modes is not unique. Conveniently, one can always choose a set of normal modes $(\tilde{Q}_{\kappa}, \tilde{P}_{\kappa})$ such that all $\text{Tr}[\tilde{I}_{kj} \rho_{AB}(0)] = 0$, which in turn leads to $\beta_{kj} = 0$ [73]. With such a choice of normal modes, the GGE again takes the form given in Eq. (13), now depending on the charges \tilde{I}_{kj} only indirectly, through the conditions $\text{Tr}[\tilde{I}_{kj} \rho_{AB}(0)] = 0$. We follow this procedure in our numerics whenever the system has a degenerate normal frequency spectrum.

In our numerical experiments, only the [2D, FB] configuration yields degenerate normal frequency spectra. In all other configurations, the spectrum is always nondegenerate. This might be related to the fact that [2D, FB] is the only configuration for which AB is effectively three dimensional (3D) (cf. Fig. 2).

That the local equilibrium of harmonic systems is described by the GGE has been established in the literature

for the following two scenarios: (i) the normal frequency spectrum must be nondegenerate but the range of interactions can be arbitrary [68]; and (ii) the normal frequency spectrum can be degenerate but the interactions must be of finite range or decaying exponentially [69,73,74]. Sure enough, our numerics confirm that the GGE describes the equilibrium for [1D, EE], [1D, FB], and [2D, EE] $\forall \alpha$ (the h_κ 's are sufficient) and for [2D, FB] with $\alpha = \infty$ (the I_{kj} 's have to be accounted for).

However, the [2D, FB] configuration with $\alpha < 2$, where the normal-frequency spectrum is degenerate and the interactions are of long range, is not covered by any of the known results about harmonic systems. For this case, we establish that the equilibrium is still described by the GGE that accounts for the charges I_{kj} . Figure 9(b) illustrates such a situation on the example of a [2D, FB] lattice with long-range interactions ($\alpha = 1$).

VI. TWO-TEMPERATURE MODEL AND G-LOCALITY

Let us now discuss the implications of g-local thermal-ity for the two-temperature model (TTM) in the strong-coupling regime. The TTM is widely used in solid-state physics [21–26,75,76] to describe a setting similar to ours. Namely, it concerns the joint thermalization of two macroscopic systems that start at different temperatures. Usually one of the systems—say, A —is a free-electron gas while the other, B , is a crystal lattice. However, the TTM is not specific to those systems and can be formulated generally, based on two assumptions.

First, the TTM posits that each system, A and B , can be described by a thermal state at all times. In our notation, that would mean that the reduced states must be global Gibbs states throughout, $\rho_A(t) = \tau(T_A(t), H_A)$ and $\rho_B(t) = \tau(T_B(t), H_B)$, where the temperatures $T_A(t)$ and $T_B(t)$ vary in time. The second assumption made by the TTM (and many of its generalizations) concerns the energy exchange between A and B . It assumes that the energy exchange is governed by a rate equation, with rates given by a Fourier-like law [21–27,76]. In Appendix G, we write this rate equation explicitly and show that its validity is equivalent to the assumption that the temperatures of the systems, $T_A(t)$ and $T_B(t)$, are differentiable functions of time that converge monotonically. Thus, the second assumption can be neatly summarized as “ $T_A(t)$ and $T_B(t)$ monotonically approach the same value T^{eq} .” The standard regime of validity of the TTM is when A and B interact relatively weakly, whereas at strong couplings it is known to break down [28].

Two key applications of the TTM are noteworthy here. First, it allows us to determine the equilibrium temperature

T^{eq} [21–23,29,30,77] which is fixed by energy conservation, i.e.,

$$\langle H_A \rangle_{T_A} + \langle H_B \rangle_{T_B} = \langle H_A \rangle_{T^{\text{eq}}} + \langle H_B \rangle_{T^{\text{eq}}}, \quad (16)$$

where $\langle H_X \rangle_T := \text{Tr}[H_X \tau(T, H_X)]$ and T_X is the initial temperature of X . The lack of accounting for the energy stored in the interaction H_{int} is a manifestation of the weak-coupling assumption. Second, the rate equation allows us to infer the temporal changes of the temperatures and energies of the interacting systems A and B [22]. This has been used to understand the ablation of metals following ultrashort pulses [78] and to characterize the ultrafast heat transport between electrons and phonons in multilayers [29]. Extensions to a three-temperature model which includes their interaction with spins have proven useful in the study of ultrafast demagnetization processes [79–81].

Based on our findings for harmonic lattices, we can now comment on the validity of the TTM beyond the weak-coupling limit for which it was originally intended. The electron–phonon setting of the original TTM corresponds to the FB coupling scenario in our setup. In Fig. 5, we see that both A and B move away from Gibbs states very quickly, even at fairly weak couplings. Hence, they have no well-defined global temperatures. This breakdown of all-time global Gibbsianity beyond the regime of extremely weak coupling is not unexpected [28,81,82].

What is perhaps surprising is that here we find that *it is possible* to associate g-local temperatures [see Eq. (5)] with A and B at *all times* (see Figs. 4 and 8). In this sense, the first assumption of the TTM can be rescued at strong coupling. Moreover, our finding that all-time g-local thermal-ity also holds in the presence of temperature gradients (see Appendix D) opens up the possibility of upgrading even the more general diffusive TTM [22,26,30,83] to the strong-coupling regime. The latter posits “local thermal equilibrium” within each lattice, i.e., that each small localized subsystem of the lattice is in a Gibbs state with respect to its own bare Hamiltonian [19,30]. Of course, when there is strong coupling within the lattice, the local thermal-ity hypothesis breaks down, whereas the g-local thermal-ity is maintained.

Regarding the second assumption of the TTM, we find that its main proposition no longer holds for harmonic lattices, even for the extended notion of g-local temperatures. This is evidenced by Figs. 4 and 8, which clearly show that $T_A^{\text{eff}}(t) - T_B^{\text{eff}}(t)$ is not monotonic in t . Therefore, beyond the weak-coupling limit, no TTM-type rate equation exists that would describe the time evolution of T_A^{eff} and T_B^{eff} . This is so despite the fact that heat capacities are well defined for both A and B because they are g-locally thermal (see the discussion in Appendix B).

Nevertheless, we find that the predictive power of Eq. (16) is partially retained for harmonic lattices. Indeed, although T_A^{eff} and T_B^{eff} may, in general, converge to two

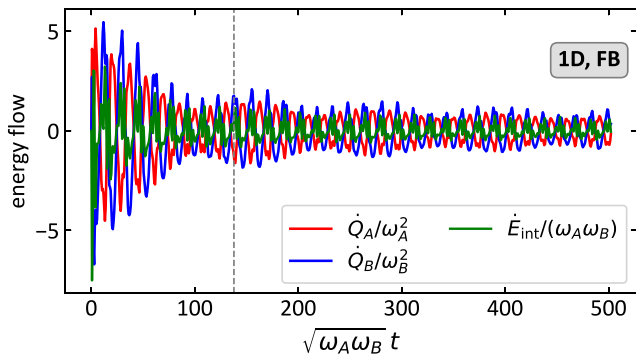


FIG. 10. Energy flows. The heat flows to each global system, $\dot{Q}_X := d\text{Tr}[H_X \rho_X]/dt$, and the interaction energy flow, \dot{E}_{int} , as functions of time. All parameters are as in Fig. 9(a). Note that the direction of the heat flow from $A \rightarrow B$ and from $B \rightarrow A$ is oscillatory. Moreover, due to the eventual equilibration of the whole system, all energy flows slowly converge to near-zero values as time goes on beyond what is shown in the plot. This plot represents generic behavior for all four geometries in Fig. 2. The vertical dashed line is chosen at $\sqrt{\omega_A \omega_B} t_{\text{bf}} \approx 137.87$, where heat back flow occurs: A has a lower temperature than B but loses heat ($\dot{Q}_A < 0$) while B receives heat ($\dot{Q}_B > 0$).

different values (see Figs. 4 and 8), Eq. (16) remains fairly accurate, with T^{eq} substituted by $T_A^{\text{eff,eq}}$ and $T_B^{\text{eff,eq}}$ (for a detailed discussion on this, see Appendix H).

Lastly, we note that, together with the nonmonotonic convergence of temperatures, the alternating direction of the heat flow shown in Fig. 10 witnesses (but does not necessitate [84]) the non-Markovian nature of the dynamics that each system X is undergoing under the influence of the other. Moreover, in contrast to the predictions of the TTM, energy may sometimes flow from cold to hot, a phenomenon sometimes referred to as “back flow of heat.”

VII. DISCUSSION AND OUTLOOK

To summarize, going beyond the too restrictive demand of global thermality, we introduce the notions of g-local thermality and the associated g-local temperatures. These characterize local subsystems while also making reference to global Gibbs states of the many-body system. We evidence the power of these concepts on the example of a pair of harmonic lattices with varying spatial dimensions and topologies of couplings. We find compelling numerical evidence that persistent g-local thermality of A and B at transient times is a necessary condition for AB to thermalize at long times. This is true even though A and B themselves venture far from being globally thermal and it applies to lattices A and B with both short- and long-range interactions within them, as well as arbitrary coupling strengths between them. This finding adds a new “expected behavior” to the short list of known results for the transient regime in the dynamics of interacting quantum many-body

systems. Furthermore, for the equilibrium state itself, we find that it is described by the GGE for all configurations and interaction ranges. This includes the peculiar case of 2D lattices with full-body coupling (rendering AB three-dimensional), for which the normal-frequency spectrum is degenerate. Such systems have an extended algebra of conserved charges, and the GGE has to be constructed taking all those charges into account.

These results open up several new directions. As a first step, many-body systems other than harmonic lattices may be tested numerically for the presence of g-local thermality. Further ahead, analytical arguments might be constructed that can prove the presence of transient g-local thermality given long-term equilibration for either harmonic lattices or more general many-body systems. Finally, experiments with atoms in optical lattices or trapped ions may in the future test the link between transient g-local thermality and long-time equilibration [14–16,65,70,72,85–88].

In general, g-local thermality naturally fits into the framework of quantum thermometry [89,90] and strong-coupling thermodynamics [7,40–42]. Performing spatially local thermometry [89–93] measures the g-local temperature of a system irrespective of whether the system state is globally thermal or g-locally thermal (see Appendix B). Such measured records give an operational meaning to g-local temperatures. Moreover, when dealing with many-body systems with local Hamiltonians, all energetic quantities are already determined by local states. Thus, those strong-coupling thermodynamics results that are derived under the assumption of global thermality [44,94–98], will naturally extend to g-locally thermal systems. Furthermore, all-time g-local thermality may enable hydrodynamic treatment of nonequilibrium transport at strong coupling not only in the steady state [99,100] but also in the transient regime. G-local thermality may also be useful in the study of local transfer in systems with noncommuting conserved charges [101,102]. Lastly, maintained g-local thermality might lead to a type of Markovianity and local detailed balance for some observables [103] under certain conditions.

Part of the motivation for this work is to provide a microscopic justification of the TTM that is often used to interpret transient heat dynamics in condensed-matter systems. The TTM assumes that both systems remain globally thermal during the interaction, an assumption that generally fails when the coupling is not weak. For our model system, we see that some of the features of the TTM can be carried over into the strong-coupling regime, by updating the restrictive global thermality assumption to g-local thermality. However, at strong couplings, we see that the g-local temperatures of A and B relax in an oscillatory fashion and that their difference may remain nonzero. This behavior is clearly incompatible with a rate-equation ansatz for heat exchange typically applied within the TTM.

Nonetheless, the maintenance of g-local thermality and the ability to write a simple (approximate) energy condition for the equilibrium (g-local) temperatures akin to Eq. (16) provides a substantial generalization of the TTM to the strong-coupling regime. The phenomenology that we find for harmonic lattices may admittedly not be fully transposed to “hot electrons” exchanging heat with a “cold crystal lattice.” The approach we propose is, however, flexible enough to capture both kinds of subsystems that one typically encounters in condensed-matter physics: either localized in a limited spatial domain or defined by a certain set of (coarse-grained) physical observables.

ACKNOWLEDGMENTS

We thank Philipp Strasberg for interesting discussions. K.H., S.N., and J.A. are grateful for support from the University of Potsdam. J.A. gratefully acknowledges funding from the Deutsche Forschungsgemeinschaft (DFG, German Research Foundation) under Grants No. 384846402 and No. 513075417 and from the Engineering and Physical Sciences Research Council (EPSRC) (Grant No. EP/R045577/1) and thanks the Royal Society for support. Open access publication is funded by the Deutsche Forschungsgemeinschaft (DFG, German Research Foundation), Project No. 491466077.

APPENDIX A: FIDELITY AND BURES DISTANCE

In the definition given in Eq. (5), one can in principle use any metric to define the effective temperature. With any choice of metric, the resulting effective temperature will coincide with the true g-local temperature whenever the system is g-locally thermal exactly.

Since our model is Gaussian (see Appendix C), it is convenient to work with the Bures metric. It is defined as [46]

$$\mathcal{D}(\rho_1, \rho_2) := [2(1 - \sqrt{\mathcal{F}(\rho_1, \rho_2)})]^{1/2}, \quad (\text{A1})$$

where

$$\mathcal{F}(\rho_1, \rho_2) := \left(\text{Tr} \sqrt{\rho_1^{1/2} \rho_2 \rho_1^{1/2}} \right)^2 \quad (\text{A2})$$

is the quantum fidelity [46]. The reason for this preference in our case is that the fidelity can be explicitly calculated for Gaussian multimode states through their covariance matrices [104–106] [see Eqs. (C18)–(C20)].

APPENDIX B: G-LOCAL THERMALITY AND LOCAL OBSERVABLES

Let us show that by using only local observables one cannot differentiate between standard (globally) thermal and uniformly g-locally thermal states of many-body systems.

An observable O living in the Hilbert space of a lattice system X is called local if it can be written as

$$O = \sum_{s \subset X} O_s, \quad (\text{B1})$$

with each O_s acting nontrivially only on some spatially localized subsystem s containing at most k sites, for some fixed k . This means that one can write $O_s = \hat{O}_s \otimes \mathbb{I}_{X \setminus s}$, where \hat{O}_s is some operator living in the Hilbert space of s .

Now, if the state of X , ρ_X , is g-locally thermal at each s , with uniform g-local temperature T , then

$$\begin{aligned} \langle O \rangle &:= \text{Tr}_X [O \rho_X] \\ &= \sum_s \text{Tr}_X \left[\left(\hat{O}_s \otimes \mathbb{I}_{X \setminus s} \right) \rho_X \right] \\ &= \sum_s \text{Tr}_s \left[\hat{O}_s \rho_s \right] \\ &\stackrel{(*)}{=} \sum_s \text{Tr}_s \left[\hat{O}_s \text{Tr}_{X \setminus s} [\tau(T, H_X)] \right] \\ &= \sum_s \text{Tr}_X \left[\left(\hat{O}_s \otimes \mathbb{I}_{X \setminus s} \right) \tau(T, H_X) \right] \\ &= \text{Tr}_X [O \tau(T, H_X)], \end{aligned} \quad (\text{B2})$$

where in step (*) the g-locality condition in Eq. (2) is used.

In particular, this means that if H_X is local, then the effective canonical temperature $T_X^{\text{eff,can}}$ of X , defined in Eq. (8), coincides with T . Indeed, in view of Eq. (B2), we have $\text{Tr}[\rho_X H_X] = \text{Tr}[H_X \tau(T, H_X)]$. Moreover, if we define the “g-local” heat capacity of X as $d \text{Tr}[H_X \rho_X] / dT$, then it will be equal to the heat capacity of X if it were in a global thermal state at temperature T .

Note that in some cases it might happen that ρ_X is g-locally thermal also at small but spatially *delocalized* subsystems containing at most k sites. Then, the equality $T_X^{\text{eff,can}} = T_X^{\text{eff}}$ will hold even if H_X is a long-range but at most k -body interacting Hamiltonian.

Finally, we note that the effective canonical temperature $T_X^{\text{eff,can}}$ has found some use in nonequilibrium thermodynamics [107–109] and that the equality $T_X^{\text{eff,can}} = T_X^{\text{eff}}$ for g-locally thermal systems provides $T_X^{\text{eff,can}}$ with an additional thermodynamic meaning.

APPENDIX C: A SUMMARY OF HARMONIC SYSTEMS

As described in Sec. III, our model system is a harmonic lattice. Namely, it is a collection of linearly coupled oscillators, so all the Hamiltonians are quadratic. The tools for simulating and calculating many physical and information-theoretical quantities for such systems are well known and

are thoroughly described in, e.g., Refs. [56–58]. Here, we give a brief account of the main notions and formulas necessary for our purposes.

The position and momentum coordinates of a system of N oscillators are conveniently collected into a column vector in the phase space

$$\mathbf{x} = \begin{pmatrix} \mathbf{q} \\ \mathbf{p} \end{pmatrix}, \quad (\text{C1})$$

with a total of $2N$ components,

$$\mathbf{q} = (q_1, \dots, q_N)^T, \quad \mathbf{p} = (p_1, \dots, p_N)^T.$$

We call this phase-space basis the “ q - p ” basis. In this basis and in units where $\hbar = 1$, the canonical commutation relations are written as

$$[x_k, x_j] = i\Upsilon_{kj}, \quad (\text{C2})$$

where the antisymmetric matrix Υ has the symplectic form:

$$\Upsilon = \begin{pmatrix} 0 & \mathbb{I} \\ -\mathbb{I} & 0 \end{pmatrix}, \quad (\text{C3})$$

in which \mathbb{I} is the $N \times N$ identity matrix and 0 is the $N \times N$ zero matrix. [A relation similar to Eq. (C2) applies in classical mechanics but with the Poisson bracket instead of the commutator.]

In terms of the phase-space coordinates \mathbf{x} , the Hamiltonian is a quadratic form

$$H = \frac{1}{2} \mathbf{x}^T F \mathbf{x}, \quad (\text{C4})$$

where we call the symmetric matrix F the “Hamiltonian matrix.” When there is no momentum–momentum coupling in the system, F takes the form

$$F = V \oplus \mathbb{I}, \quad (\text{C5})$$

where V corresponds to the “potential energy” part of the Hamiltonian and the identity \mathbb{I} specifies the kinetic energy (after scaling out the oscillator masses).

Two harmonic systems A and B can be combined by forming the direct sum of their phase spaces, with the joint Hamiltonian matrix

$$F_{AB} = V_{AB} \oplus \mathbb{I}_{AB}, \quad (\text{C6})$$

where

$$V_{AB} = V_A \oplus V_B + V_{\text{int}}. \quad (\text{C7})$$

Here, the interaction potential V_{int} represents H_{int} that couples A and B [see, e.g., Eq. (11)].

Due to a theorem by Williamson [110], any Hamiltonian matrix can be symplectically diagonalized. Namely, there exists a symplectic transformation matrix S such that

$$S^T F S = \Omega \oplus \Omega, \quad (\text{C8})$$

where the diagonal matrix $\Omega = \text{diag}(\Omega_1, \dots, \Omega_N)$ collects the normal-mode frequencies of the system. Recall that symplectic is any matrix that leaves the canonical commutation relation in Eq. (C2) invariant: $S^T \Upsilon S = \Upsilon$.

The same matrix S switches from the q - p basis to the normal-mode basis:

$$\mathbf{x} = S \mathbf{X}, \quad (\text{C9})$$

where $\mathbf{X} = (Q_1, \dots, Q_N, P_1, \dots, P_N)^T$ collects the positions and momenta of the normal modes. In the normal-mode basis, the Hamiltonian is a sum of noninteracting oscillators:

$$H = \sum_j \Omega_j \left[\frac{Q_j^2}{2} + \frac{P_j^2}{2} \right]. \quad (\text{C10})$$

The initial state $\rho(0)$ given in Eq. (12) is a tensor product of Gibbs states of quadratic Hamiltonians; therefore, it is Gaussian. Hence, there is no net displacement of the phase-space coordinates, $\langle \mathbf{x} \rangle_t := \text{Tr}[\rho(t) \mathbf{x}] = 0$, and, since the Hamiltonian is quadratic at all times, the state $\rho(t)$ also remains Gaussian at all times [58].

Gaussian states are uniquely determined by the covariance matrix [58]

$$\sigma_{jk} = \frac{1}{2} \text{Tr}[\rho(x_j x_k + x_k x_j)], \quad (\text{C11})$$

where the curly brackets denote the anticommutator. Conveniently, the covariance matrix of any subsystem (in our case, it can be A or B or some small subsystem of sites) is simply the corresponding sub-block of σ , which determines its reduced state.

Whenever the system is in a Gibbs state [i.e., $\rho = \tau(T, H)$; see Eq. (1)], the covariance matrix in the normal-mode basis,

$$\Sigma_{jk} = \frac{1}{2} \text{Tr}[\tau(T, H)(X_j X_k + X_k X_j)], \quad (\text{C12})$$

is diagonal and given by [58]

$$\Sigma = R \oplus R, \quad (\text{C13})$$

where $R = \text{diag}(R_1, \dots, R_N)$, with

$$R_j = \frac{1}{2} \coth \frac{\Omega_j}{2T}. \quad (\text{C14})$$

Due to Eq. (C9), the covariance matrix in the “original” q - p basis x is then

$$\sigma = S\Sigma S^T. \quad (\text{C15})$$

Noting that the covariance matrix for a tensor product $\rho_A \otimes \rho_B$ is a direct sum, $\sigma_A \oplus \sigma_B$, we can thus construct the covariance matrix of the initial state given in Eq. (12).

As for calculating the dynamics of the system, they can be derived immediately from the Heisenberg equations of motion for \mathbf{x} that the evolution of the covariance matrix under a quadratic Hamiltonian is a symplectic transformation [58,111]:

$$\sigma(t) = \mathcal{E}(t)\sigma(0)\mathcal{E}(t)^T, \quad (\text{C16})$$

where $\mathcal{E}(t)$ is a symplectic matrix. Moreover, $\mathcal{E}(t)$ is explicitly expressed through the matrix F given in Eq. (C4) [112,113]. When the Hamiltonian is time independent, F is constant and

$$\mathcal{E}(t) = e^{\Upsilon Ft}. \quad (\text{C17})$$

Furthermore, to find effective g-local temperatures through Eq. (5), we need to calculate the fidelity given in Eq. (7). For two N -mode Gaussian states, ρ_1 and ρ_2 , with respective covariance matrices σ_1 and σ_2 and identical average coordinates (which are zero in our case), the fidelity is given by [106]

$$\mathcal{F}(\rho_1, \rho_2) = \left[\frac{M}{\det(\sigma_1 + \sigma_2)} \right]^{1/4}, \quad (\text{C18})$$

where

$$M = \det \left[2 \left(\sqrt{\mathbb{I} + \frac{1}{4}(C\Upsilon)^{-2} + \mathbb{I}} \right) C \right], \quad (\text{C19})$$

in which \mathbb{I} and Υ are the $(2N) \times (2N)$ identity matrix and the symplectic form [Eq. (C3)], respectively. The matrix C is defined as

$$C = -\Upsilon(\sigma_1 + \sigma_2)^{-1} \left(\frac{\Upsilon}{4} + \sigma_2 \Upsilon \sigma_1 \right). \quad (\text{C20})$$

Lastly, let us find the generalized inverse temperatures β_κ in the GGE for harmonic systems. These are determined from Eq. (15). Since all the charges h_κ live in nonoverlapping Hilbert spaces, we have

$$\text{Tr} [h_\kappa \rho_{AB}^{\text{GGE}}] = \frac{\text{Tr} [h_\kappa e^{-\beta_\kappa h_\kappa}]}{\text{Tr} [e^{-\beta_\kappa h_\kappa}]} = \frac{\Omega_\kappa}{2} \coth \frac{\beta_\kappa \Omega_\kappa}{2}.$$

Thus, equating this to $\langle h_\kappa \rangle = \text{Tr} [h_\kappa \rho_{AB}(0)]$, we find that

$$\beta_\kappa = \frac{2}{\Omega_\kappa} \text{arctanh} \frac{\Omega_\kappa}{2 \langle h_\kappa \rangle}. \quad (\text{C21})$$

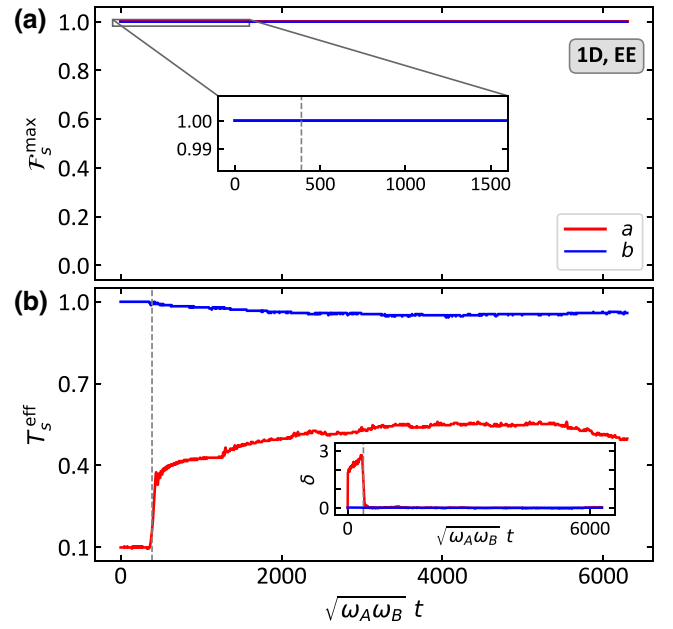


FIG. 11. The g-local thermality of A at a and B at b . (a) Similarly to Fig. 4, the fidelity \mathcal{F}_s^{\max} [see Eq. (7)] of A at $s = a$ (red) and of B at $s = b$ (blue) as a function of time t . For each X , the single-site subsystem s is located at the center of the lattice X . A and B are connected at $\nu = 1$. The inset zooms into the fidelity at early times. The fidelities remain very close to 1 (the smallest \mathcal{F}_s^{\max} being 0.999979), indicating that both A and B are g-locally thermal at a and b , respectively, with extremely good precision at all times during the evolution. (b) The corresponding effective temperatures T_s^{eff} [see Eq. (5)]. The inset is for δ —the relative discrepancy between the effective g-local and canonical temperatures. It is large in the transient regime, signaling a significant temperature gradient in the system (cf. Fig. 12). This plot is for A and B both having only nearest-neighbor interactions within them ($\alpha = \infty$). All other parameters are the same as in Fig. 4. The vertical dashed line indicates the instance at which Fig. 12 is plotted.

APPENDIX D: G-LOCAL THERMALITY FOR EDGE-EDGE COUPLED LATTICES

EE coupling is present when the interaction Hamiltonian is of the form

$$H_{\text{int}}^{(\text{EE})} = \lambda \sum_{\nu \in \text{edge}} q_{A,\nu} q_{B,\nu}, \quad (\text{D1})$$

where ν runs over the sites located on the interacting edge of each lattice (for an illustration, see the left column of Fig. 2).

For example, when A and B are 1D, the edge consists of a single site. For such a configuration, with A and B featuring nearest-neighbor interactions, the dynamics of the fidelity \mathcal{F}_s^{\max} and effective g-local temperature T_s^{eff} of a single-site subsystem s located at the center of X are

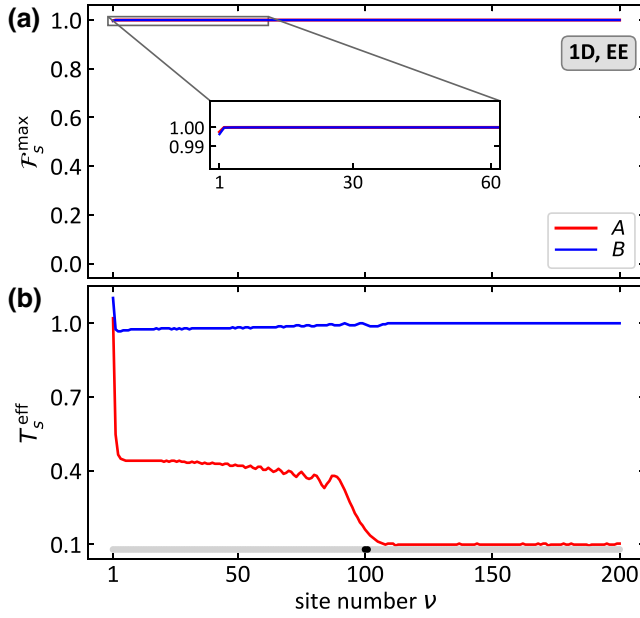


FIG. 12. The g-local thermality with site number ν . (a) Similarly to Fig. 6, the fidelity \mathcal{F}_s^{\max} [see Eq. (7)] of A at single-site subsystem $s = a$ (red) and of B at $s = b$ (blue), respectively, as a function of the site number ν . (b) The corresponding effective temperatures T_s^{eff} [see Eq. (5)] as a function of the site number ν . Here, ν labels *all* single-site subsystems s in X , with $\nu = 1, \dots, N$. We see that the fidelities \mathcal{F}_s^{\max} are very close to 1 for all ν (the smallest \mathcal{F}_s^{\max} being 0.996439). However, in contrast to the [1D, FB] case shown in Fig. 6, the g-local temperatures T_s^{eff} change with s —there is a (g-local) temperature gradient in the system. The “slider” (black dot) at the bottom indicates the position of the subsystem s in X at which Fig. 11 is plotted. Here, $\sqrt{\omega_A \omega_B} t_0 \approx 389.71$ and all other parameters are as in Fig. 11.

plotted in Fig. 11. Similarly to the case of FB coupling discussed in Sec. IV, we see that s remains g-locally thermal at all times to a good approximation.

We also note in Fig. 11(b) that the effective temperature of s remains unchanged for some time. This happens because the speed of sound in each system is finite and therefore it takes a finite amount of time for the perturbation caused by switching on the coupling at the edge to reach the center of the chain (where s is located).

For this very reason, there is also a temperature gradient within each lattice X in the transient regime, before the total system equilibrates. A snapshot of that is presented in Fig. 12, where the fidelity \mathcal{F}_s^{\max} and effective g-local temperature T_s^{eff} are plotted as a function of the position of a single-site subsystem s that slides along the chain (just as in Fig. 6). Here, we see that while all s are g-locally thermal to an excellent approximation, their temperature now depends on the position of s . Due to this gradient, the effective canonical temperature given in Eq. (8) becomes inadequate, as is emphasized in the inset of Fig. 11(b).

Expectedly, at those times when there is a temperature gradient in the lattices, the decay of \mathcal{F}_s^{\max} with N_s is faster as compared with the FB case. Moreover, even small (e.g., $N_s = 2$) but delocalized subsystems s (i.e., when $s = \{\nu_1, \nu_2\}$ with, e.g., $\nu_1 = 50$ and $\nu_2 = 150$), are no longer g-locally thermal. This contrasts with the [1D, FB] and [2D, FB] cases, where all small subsystems, localized or not, are g-locally thermal to a good approximation.

APPENDIX E: NUMERICAL DEMONSTRATION OF THE MAIN RESULT

In this appendix, we numerically demonstrate the validity of our main result laid out in Sec. IV (and illustrated in Fig. 3). It states that g-local thermality of A and B is guaranteed *at all times, including during the transient*, whenever all local observables of AB equilibrate dynamically at long times.

We first describe the parameter space and then discuss the relevant figures of merit and show pertinent results of our simulations.

1. Parametrization

A natural dimensionless parametrization of the system and its dynamics can be achieved as follows. First, we recall that we work in the natural units where $\hbar = k_B = 1$ and the masses of all the oscillators are set to 1. Therefore, the transformation $\tilde{q} = q\sqrt{\omega}$, $\tilde{p} = p/\sqrt{\omega}$ renders \tilde{q} and \tilde{p} dimensionless while preserving the canonical commutation relations. In these terms,

$$H_X = \omega_X h_X(\tilde{q}_\nu, \tilde{p}_\nu, \tilde{g}_X, \alpha), \quad (\text{E1})$$

where the dimensionless operator function h_X of the dimensionless quantities $(\tilde{q}_\nu, \tilde{p}_\nu, \tilde{g}_X, \alpha)$, with

$$\tilde{g}_X := g_X / \omega_X^2, \quad (\text{E2})$$

is given by

$$h_X = \frac{1}{2} \sum_\nu (\tilde{q}_\nu^2 + \tilde{p}_\nu^2) + \sum_{\nu \neq \nu'} \tilde{G}_X^{\nu, \nu'} \tilde{q}_{X, \nu} \tilde{q}_{X, \nu'}. \quad (\text{E3})$$

Here, by natural extension of Eq. (10),

$$\tilde{G}_X^{\nu, \nu'} := \frac{\tilde{g}_X}{\text{dist}(\nu, \nu')^\alpha}. \quad (\text{E4})$$

Introducing the dimensionless lattice–lattice coupling

$$\tilde{\lambda} := \lambda / (\omega_A \omega_B) \quad (\text{E5})$$

and

$$\mu := \sqrt{\omega_A / \omega_B}, \quad (\text{E6})$$

we obtain the total Hamiltonian

$$H_{\text{tot}} = \sqrt{\omega_A \omega_B} h_{\text{tot}}, \quad (\text{E7})$$

where, for e.g., the FB coupling, the dimensionless operator h_{tot} is

$$h_{\text{tot}} = \mu h_A + \mu^{-1} h_B + \tilde{\lambda} \sum_v \tilde{q}_{A,v} \tilde{q}_{B,v}. \quad (\text{E8})$$

As mentioned in Sec. III, in the five-dimensional system-parameter space with coordinates $(\mu, \alpha, \tilde{\lambda}, \tilde{g}_A, \tilde{g}_B)$, the set of allowed system parameters is determined by the condition that the operator h_{tot} is unbounded from below.

Lastly, the evolution in dimensionless time

$$\tilde{t} := t \sqrt{\omega_A \omega_B} \quad (\text{E9})$$

is generated by

$$U = e^{-i\tilde{t} h_{\text{tot}}} \quad (\text{E10})$$

and defining the dimensionless temperatures as

$$\tilde{T}_X := T_X / \omega_X, \quad (\text{E11})$$

we can express the initial state given in Eq. (12) in terms of dimensionless quantities:

$$\rho_{AB}(0) \propto e^{-h_A/\tilde{T}_A} \otimes e^{-h_B/\tilde{T}_B}. \quad (\text{E12})$$

2. Relevant quantities and data

Although we formulate our all-time g-local thermality result in a “discrete” true–false language (see Fig. 3), there is more quantitative structure to the dependence of the degree of g-local thermality on the degree of long-time equilibration. To properly showcase this relationship, we need a quantification of both phenomena.

First, we pick a long enough time interval $[0, \tilde{t}_m]$ over which we observe the system. Then, since we already have a well-defined measure of g-local thermality at an instant of time \tilde{t} and subsystem s , $\mathcal{F}_s^{\text{max}}(\tilde{t})$, we use it to introduce a measure of all-time (AT) g-local thermality at s , defined as

$$\mathcal{F}_s^{\text{AT}} = \min_{\tilde{t} \in [0, \tilde{t}_m]} \mathcal{F}_s^{\text{max}}(\tilde{t}). \quad (\text{E13})$$

To quantify the degree to which the system locally equilibrates as per the definition in Sec. V, we employ the fact that, if equilibration occurs, then it is described by the GGE in the thermodynamic limit (see Sec. V). The main quantifier here is the longest “equilibrium interval” during the $[0, \tilde{t}_m]$ period. By an equilibrium interval, we mean any $[\tilde{t}_i^{\text{eq}}, \tilde{t}_f^{\text{eq}}]$ such that $\mathcal{D}[\rho_s(\tilde{t}), \rho_s^{\text{GGE}}] \leq \epsilon \forall \tilde{t} \in [\tilde{t}_i^{\text{eq}}, \tilde{t}_f^{\text{eq}}]$.

The figure of merit that we use is the ratio of the longest equilibrium interval,

$$\tau_s^{\text{eq}} := \max_{[\tilde{t}_i^{\text{eq}}, \tilde{t}_f^{\text{eq}}] \subset [0, \tilde{t}_m]} (\tilde{t}_f^{\text{eq}} - \tilde{t}_i^{\text{eq}}), \quad (\text{E14})$$

to the total duration of observation:

$$r_s^{\text{eq}} = \frac{\tau_s^{\text{eq}}}{\tilde{t}_m}. \quad (\text{E15})$$

In parallel with r_s^{eq} , we use the average distance from equilibrium,

$$\langle \mathcal{D}_s \rangle = \frac{1}{\tilde{t}_m} \int_0^{\tilde{t}_m} d\tilde{t} \mathcal{D}[\rho_s(\tilde{t}), \rho_s^{\text{GGE}}], \quad (\text{E16})$$

to quantify the local equilibration.

The quantity $\langle \mathcal{D}_s \rangle$ cannot be used alone to “measure” equilibration, as even a very small value of $\langle \mathcal{D}_s \rangle$ does not exclude frequent ϵ -surpassing peaks of $\mathcal{D}[\rho_s(\tilde{t}), \rho_s^{\text{GGE}}]$. Similarly, used alone, r_s^{eq} indicates the time that \mathcal{D}_s uninterruptedly spends under ϵ but does not tell us how much lower than ϵ it typically gets. So, although r_s^{eq} and $\langle \mathcal{D}_s \rangle$ are not independent (e.g., if $r_s^{\text{eq}} = 1$, then necessarily $\langle \mathcal{D}_s \rangle \leq \epsilon$), only when considering them together does one get a complete picture of how well AB locally equilibrates at s —one needs a small $\langle \mathcal{D}_s \rangle$ and a large r_s^{eq} to ensure equilibration.

Regarding the choice of \tilde{t}_m , we note that although verifying equilibration is in general an undecidable problem [114], the situation in quadratic harmonic systems is more predictable. Indeed, as discussed in Sec. V, if equilibration occurs, then the equilibrium is described by the GGE. Moreover, it has been shown in Ref. [74] that if the interactions in the system are of short range, then the equilibration time does not depend on the system size and the recurrence time grows linearly with the size. For systems with long-range interactions, our numerical experiments show that the pattern is similar—if the system equilibrates, it does so relatively quickly; and if it does not, then local states show no tendency to converge at long times. For the plots in Figs. 13–15, we find $\tilde{t}_m = 10\,000$ to be sufficiently long, yet not too long for recurrences to significantly affect the picture.

In terms of the above-introduced quantities, the claim in our main result is as follows (for a recap, see Fig. 3). If r_s^{eq} is small *or* $\langle \mathcal{D}_s \rangle$ is large (i.e., poor equilibration), then $\mathcal{F}_s^{\text{AT}}$ can be anything. If r_s^{eq} is close to 1 *and* $\langle \mathcal{D}_s \rangle$ is small (i.e., good equilibration), then $\mathcal{F}_s^{\text{AT}}$ has to be close to 1.

This is indeed what we see numerically. We have explored the full parameter range by both randomly sampling the parameters $(\mu, \alpha, \tilde{\lambda}, \tilde{g}_A, \tilde{g}_B, \tilde{T}_A, \tilde{T}_B)$ and deliberately choosing values at the boundaries of the set of allowed parameters (determined by the condition that the total Hamiltonian is nonnegative; see Appendix E 1).

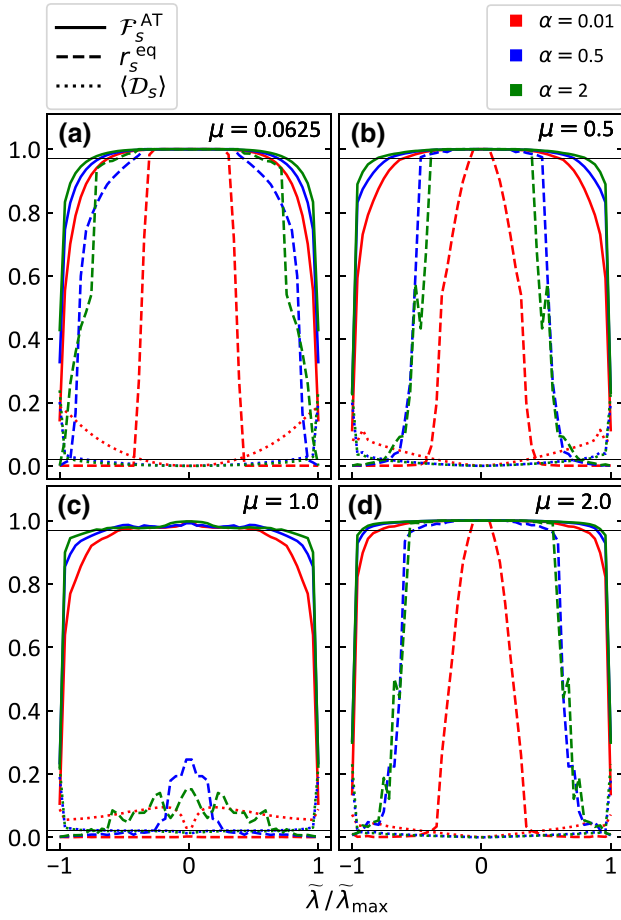


FIG. 13. The degrees of all-time g-local thermality and long-time equilibration versus $\tilde{\lambda}$: (a) $\mu = 0.0625$; (b) $\mu = 0.5$; (c) $\mu = 1.0$; (d) $\mu = 2.0$. Each panel shows $\mathcal{F}_s^{\text{AT}}$ (solid line), r_s^{eq} (dashed line), and $\langle \mathcal{D}_s \rangle$ (dotted line) as functions of $\tilde{\lambda}$. The different colors correspond to different values of α . The upper horizontal line is at 0.97 and represents the threshold value of $\mathcal{F}_s^{\text{AT}}$ above which we say that the system is g-locally thermal at all times. The lower horizontal line is the $\epsilon = 0.02$ threshold for $\langle \mathcal{D}_s \rangle$. The configuration is [1D, FB] and the plots are for the central two-node subsystem of A . The other parameters are $N_A = N_B = 200$, $\tilde{g}_A = 0.2$, $\tilde{g}_B = 0.3$, $\tilde{T}_A = 0.1$, and $\tilde{T}_B = 1$. The $\mu = 1$ ($\omega_A = \omega_B$) case is distinctive in that the equal frequencies result in resonant oscillations that give rise to periodic spikes in $\mathcal{D}[\rho_s(t), \rho_s^{\text{GGE}}]$, resulting in poor equilibration. Nonetheless, the system experiences all-time g-local thermality to a good extent. Viewing the plot from $\tilde{\lambda} = 0$, we see that the quality of equilibration deteriorates much faster than the degree of all-time g-local thermality as $\tilde{\lambda}$ approaches $\pm\tilde{\lambda}_{\max}$ —the maximal value of $|\tilde{\lambda}|$ for which H_{tot} is bounded from below.

Since the parameter space is seven-dimensional (not counting N_A , N_B , and the configuration of lattice-lattice interaction) and therefore impossible to draw, we present our results in two-dimensional cross sections.

In our numerical experiments, we found that there are three “dangerous” parameter regimes. The first is

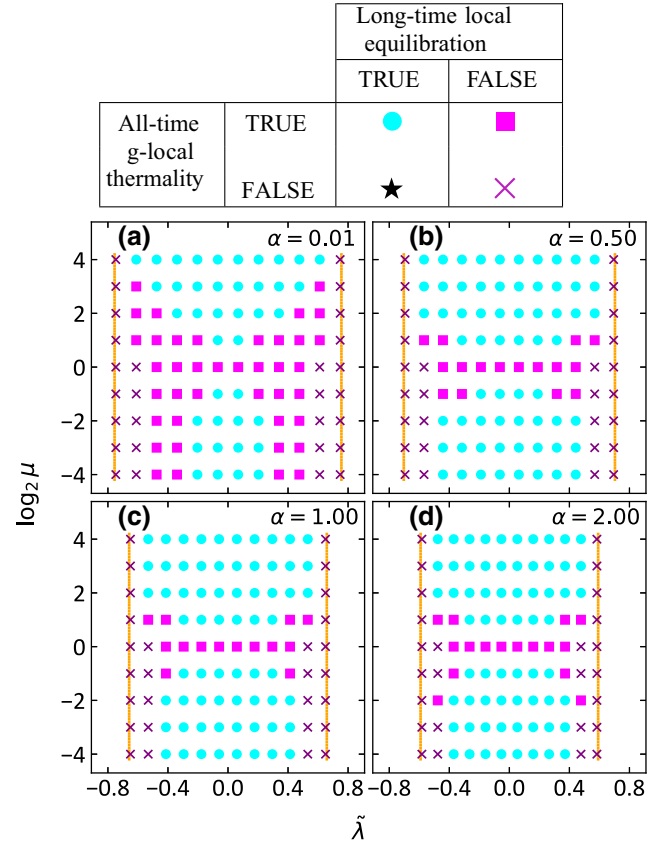


FIG. 14. The all-time g-local thermality and long-time local equilibration versus $\tilde{\lambda}$ and μ . Each panel shows whether or not all-time g-local thermality and long-time equilibration occur, as per the color and shape coding in the table, as a function of $\tilde{\lambda}$ and μ . The panels are for four different values of α : (a) $\alpha = 0.01$; (b) $\alpha = 0.50$; (c) $\alpha = 1.00$; (d) $\alpha = 2.00$. All other parameters are fixed to the same values as in Fig. 13. The orange lines are at $\pm\tilde{\lambda}_{\max}$, marking the boundary of the set of all $(\tilde{\lambda}, \mu)$ for which H_{tot} is bounded from below. Here, the TRUE threshold for all-time g-local thermality is chosen to be $\mathcal{F}_s^{\text{AT}} \geq 0.97$ for all subsystems s of size 2. For long-time equilibration, the TRUE threshold is $\min_{|s|=2} r_s^{\text{eq}} \geq 0.8$ and $\max_{|s|=2} \langle \mathcal{D}_s \rangle \leq \epsilon = 0.02$. We see that all combinations occur except the ★, in accordance with the claim in the main text (see also Fig. 3). The table shows the shape and color coding of the four logical possibilities for observing or not observing all-time g-local thermality and long-time local equilibration used in the plot.

strong A/B frequency imbalance: $\mu \ll 1$ or $\mu \gg 1$. The other parameter that has a significant effect on the g-local-thermality–equilibration relation is α —the range of intralattice interactions. Indeed, as we see in Appendix F, canonical-typicality–based results become inapplicable for small values of α , making the regime of small α ’s also dangerous. The third is the regime of strong lattice–lattice coupling, which also bears the potential to be dangerous, as both A and B lose their dynamic individuality when $\tilde{\lambda}$ is

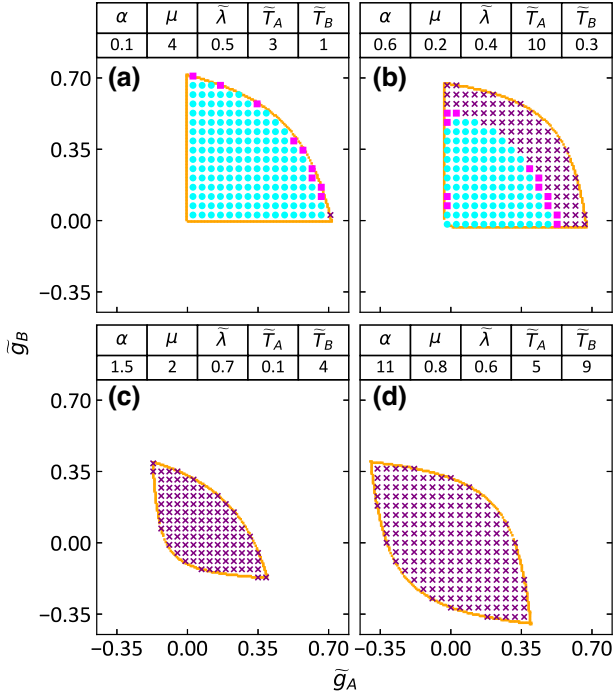


FIG. 15. The all-time g-local thermality and long-time local equilibration versus \tilde{g}_A and \tilde{g}_B . Each panel shows whether or not all-time g-local thermality and long-time equilibration occur, as per the color and shape coding in the table in Fig. 14, as a function of \tilde{g}_A and \tilde{g}_B : (a)–(d) are for four different sets of parameters $(\alpha, \mu, \tilde{\lambda}, \tilde{T}_A, \tilde{T}_B)$, as shown at the top of each panel. As previously, $N_A = N_B = 200$ and the configuration is [1D, FB]. In each panel, the orange border outlines the set of all $(\tilde{g}_A, \tilde{g}_B)$ such that H_{tot} is bounded from below. As in Fig. 14, here the TRUE threshold for all-time g-local thermality is $\min_{|s|=2} \mathcal{F}_s^{\text{AT}} \geq 0.97$ and for long-time equilibration, the TRUE threshold is $\min_{|s|=2} r_s^{\text{eq}} \geq 0.8$ and $\max_{|s|=2} \langle \mathcal{D}_s \rangle \leq \epsilon = 0.02$. We see that all combinations occur except the \star , in accordance with the claim illustrated in Fig. 3. The lack of all-time g-local thermality and equilibration in (c) and (d) is consistent with Fig. 13: in both (c) and (d), $\tilde{\lambda}/\tilde{\lambda}_{\text{max}}$ is close to 1.

large, especially in the FB coupling configuration. Therefore, our emphasis in the numerical exposition below will be on cross sections of μ , α , and $\tilde{\lambda}$. Note that large $\tilde{\lambda}$ means that $|\tilde{\lambda}|$ is close to $\tilde{\lambda}_{\text{max}}$, which is the maximal value of $|\tilde{\lambda}|$ (with all other parameters fixed) for which H_{tot} is bounded from below.

The most insight is provided by Fig. 13, where we plot the degrees of all-time g-local thermality ($\mathcal{F}_s^{\text{AT}}$) and equilibration (r_s^{eq} and $\langle \mathcal{D}_s \rangle$) as functions of $\tilde{\lambda}$, for different (extremal and not) values of α and μ . There, we see that the quality of equilibration deteriorates significantly faster than the degree of all-time g-local thermality as $|\tilde{\lambda}|$ approaches its maximum ($\tilde{\lambda}_{\text{max}}$). This confirms our claim and, in a way, makes the relation between all-time g-local thermality and long-time equilibration more quantitative.

A different cross section of the $(\mu, \alpha, \tilde{\lambda})$ subset is presented in Fig. 14. There, we plot all-time g-local thermality and long-time local equilibration in a discrete fashion: occurs (TRUE) or does not occur (FALSE). The four logical possibilities are presented in the table in Fig. 14, with corresponding color and shape coding. Now, the claim of our main result, as formulated in Sec. IV and summarized in Fig. 3, is that the combination [all-time g-local thermality = FALSE] and [long-time local equilibration = TRUE], encoded as \star , never occurs. And, indeed, we see no \star in Fig. 14.

Figure 15 is another TRUE–FALSE plot, this time across four \tilde{g}_A – \tilde{g}_B planes, each corresponding to a panel of the plot. The values of the parameters fixing the planes are presented above the panels. In Fig. 15(a), we have A with much larger initial energy and heat capacity ($\omega_A = 16 \omega_B$ and $T_A = 48 T_B$) and so, expectedly, the evolution does not perturb it much, so its g-local thermality is largely maintained even at the edge of the parameter space. In Fig. 15(b), A has a much smaller heat capacity than B ($\omega_A = \omega_B/25$) and starts at a similar temperature with B ($T_A \approx 1.33 T_B$), so we see more diversity of options. In Figs. 15(c) and 15(d), the respective $\tilde{\lambda}$'s are close to their maximal values and so, as could be anticipated from Fig. 13, we observe that neither all-time g-local thermality nor long-time local equilibration occur to a high enough degree.

We observe the picture described above over all cross sections of the parameter set, for all configurations and spatial dimensions. We take this as compelling numerical proof of our main result.

APPENDIX F: COMPARISON WITH ENSEMBLE EQUIVALENCE

By the stronger equivalence of ensembles, we mean Ref. [50, Proposition 2]. In a slightly simplified form derived in Ref. [55] (Lemma 2), it states the following. Say, X is a d -dimensional (hyper)cubic lattice with $N = n^d$ sites. Each site contains a quantum system described by a finite-dimensional Hilbert space, with the dimension being the same for all sites. The Hamiltonian is of finite range (i.e., local, as per the definition in Appendix B): $H_X = \sum_{v \in X} h_v$, with h_v acting only on sites v' with $\text{dist}(v, v') \leq k$. Now, let τ_X be a state with exponentially decaying correlations and fix some $0 < c < 1/(d+2)$. If

$$S(\rho_X \| \tau_X) = o(N^{\frac{1-c(d+2)}{d+1}}), \quad (\text{F1})$$

where $S(\rho \| \tau) := \text{Tr}[\rho(\ln \rho - \ln \tau)]$ is the relative entropy, then [50,55]

$$\mathbb{E}_{s \in C_l} \|\rho_s - \tau_s\|_1 = O(N^{-c/2}), \quad (\text{F2})$$

where $\|\mathcal{D}\|_1 := \text{Tr} \sqrt{\mathcal{D}^\top \mathcal{D}}$ is the trace norm, C_l is the set of all subhypercubes s of X with side length

$$l = o(n^{\frac{1-c}{d+1}}) \quad (\text{F3})$$

and $\mathbb{E}_{s \in C_l}$ denotes arithmetic averaging over C_l . Namely,

$$\mathbb{E}_{s \in C_l} \|\rho_s - \tau_s\|_1 := \frac{1}{K_l} \sum_{s \in C_l} \|\rho_s - \tau_s\|_1, \quad (\text{F4})$$

where K_l is the size of C_l (i.e., the amount of subhypercubes s in it). Here, the big O and small o are as per the standard asymptotic notation and, as in the main text, $\rho_s := \text{Tr}_{X \setminus s}[\rho_X]$.

In simple terms, this lemma means that if τ_X has exponentially decaying correlations and ρ_X is not very far from it in terms of the relative entropy [Eq. (F1)], then ρ_X is locally close to τ_X , in trace norm, for almost all small subsystems [Eq. (F2)]. Here, “small” refers to any subsystem the diameter of which is $o(n^{(1-c)/(d+1)})$ [Eq. (F3)]; of course, any fixed size is $o(n^{(1-c)/(d+1)})$ in the thermodynamic limit.

To translate Eq. (F2) into a statement about the Bures distance, note that, in view of the Fuchs–van de Graaf inequality [115], $\mathcal{D}[\rho, \tau]^2 \leq \|\rho - \tau\|_1$. Therefore,

$$\begin{aligned} \mathbb{E}_{s \in C_l} \mathcal{D}[\rho_s, \tau_s] &= \frac{1}{K_l} \sum_{s \in C_l} \mathcal{D}[\rho_s, \tau_s] \\ &\stackrel{(*)}{\leq} \frac{1}{K_l} \sqrt{\sum_{s \in C_l} 1^2} \sqrt{\sum_{s \in C_l} \mathcal{D}[\rho_s, \tau_s]^2} \\ &\leq \sqrt{\frac{1}{K_l} \sum_{s \in C_l} \|\rho_s - \tau_s\|_1}, \end{aligned}$$

where the step (*) is due to the Cauchy–Schwarz inequality. Hence, in view of Eq. (F2), we find that

$$\mathbb{E}_{s \in C_l} \mathcal{D}[\rho_s, \tau_s] = O(N^{-c/4}). \quad (\text{F5})$$

Coming back to our setup, let $\rho_X(t)$ be the state of the lattice X at the moment of time t and let $T_X^{\text{eff,can}}(t)$ be its effective canonical temperature, as per the definition in Eq. (8). Also, let

$$\tau_X^{\text{eff,can}}(t) := \tau(T_X^{\text{eff,can}}(t), H_X) \quad (\text{F6})$$

be the Gibbs state corresponding to it. Now, observing that, due to Eq. (8),

$$S(\rho_X(t) \| \tau_X^{\text{eff,can}}(t)) = S(\tau_X^{\text{eff,can}}(t)) - S(\rho_X(t)),$$

where $S(\rho)$ is the von Neumann entropy, and keeping in mind Eqs. (F5) and (2), we can state the following consequence of Refs. [50, Proposition 2] and [55, Lemma 2].

Corollary 1 (of Proposition 2 of Ref. [50]).—If $\tau_X^{\text{eff,can}}(t)$ has exponentially decaying correlations and

$$S(\tau_X^{\text{eff,can}}(t)) - S(\rho_X(t)) = o(N^{\frac{1-c(d+2)}{d+1}}), \quad (\text{F7})$$

then $\rho_X(t)$ is g -locally thermal at (almost) uniform temperature $T_X^{\text{eff,can}}(t)$, up to a correction $\propto N^{-c/4}$. The g -local thermality of X is at the level of subsystems of diameter $l = o(n^{(1-c)/(d+1)})$ [Eq. (F3)].

This result provides a background against which we can assess how “expected” the all-time g -local thermality result in Sec. IV is for short-range Hamiltonians. Indeed, when H_X is finite ranged and gapped, $\tau(T, H_X)$ has exponentially decaying correlations at any T [116]. So, the first condition of Corollary 1 is satisfied.

The validity of the second condition is, in general, much harder to assess *a priori*. But given that the entropy difference in Eq. (F7) is zero at $t = 0$ in our setting, it would not be too surprising if it were to remain small enough to never violate Eq. (F7) during the evolution. This is so especially when H_{int} is invariant under translations in X (e.g., FB coupling), since in that case, one expects that both $\tau_X^{\text{eff,can}}(t)$ and $\rho_X(t)$ will remain translationally invariant (except for the edges) at all times.

We emphasize that Corollary 1 has no bearing on the degree of validity of the condition given in Eq. (F7). Thus, it does *not* prove all-time g -local thermality of X when H_X is short ranged and gapped and H_{int} is translationally invariant. However, Corollary 1 does show that it is not unexpected that we do observe all-time g -local thermality for such systems. In fact, when A and B are FB-coupled 2D lattices with nearest-neighbor interactions, we see in the bottom inset of Fig. 8 that g -local thermality is accompanied by $T_X^{\text{eff}}(t) \approx T_X^{\text{eff,can}}$ at all times. This suggests (but does not prove) that Corollary 1 applies in this case.

The situation changes, even for short-ranged H_X , when H_{int} is not translationally invariant; e.g., in the case of EE coupling. Then, due to the gradients of energy (and temperature), the condition in Eq. (F7) becomes unlikely to be satisfied at all times. By directly looking at $\mathbb{E}_{s \in C_l} \mathcal{D}[\rho_s, \tau_s]$, we indeed see that Eq. (F5) is violated. Let us consider, for concreteness, the [1D, EE] case for which Fig. 12 is plotted. Each single-site subsystem is almost exactly g -locally thermal, so, noting that C_1 is simply the set of all sites of X , we can write

$$\mathbb{E}_{s \in C_1} \mathcal{D}[\rho_s, \tau_s] = \frac{1}{N} \sum_{v=1}^N \mathcal{D}[\tau_v^{\text{MF}}(T_v^{\text{eff}}), \tau_v^{\text{MF}}(T_X^{\text{eff,can}})].$$

And since almost half of the sites of A are at $T_v^{\text{eff}} \approx 0.5$ and the other approximately 25% are at $T_v^{\text{eff}} \approx 0.1$, there exists some $\zeta > 0$ such that $\sum_{v=1}^N \mathcal{D}[\tau_v^{\text{MF}}(T_v^{\text{eff}}), \tau_v^{\text{MF}}(T_X^{\text{eff,can}})] \geq N\zeta$. Hence, $\mathbb{E}_{s \in C_1} \mathcal{D}[\rho_s, \tau_s] \geq \zeta$ and therefore Eq. (F5)

cannot hold for $N \gg 1$. Thus, Corollary 1 does not apply. Nonetheless, both A and B remain g-locally thermal at all times, with very high accuracy, as Figs. 11 and 12 clearly illustrate.

Even further from the scope of Ref. [50], and consequently of Corollary 1, are lattices with long-range interactions. In such systems, ensemble equivalence is known to generally fail [117,118]. It is, however, worth noting that, in Ref. [52], it is proven that, for long-range interacting systems, microcanonical and canonical ensembles become equivalent at high temperatures. However: (i) that result is only for microcanonical and canonical states, not for general states like Proposition 2 of Ref. [50], so it cannot be used in our scenario; and (ii) for the values of interaction range $\alpha \leq d$, the threshold temperature above which the ensemble equivalence is established in Ref. [52] diverges with N . In contrast, our all-time g-local thermality result holds for long-range interacting systems with arbitrary α (Figs. 4 and 6 illustrate that for $\alpha = 0.5$).

That the ensemble equivalence fails, whereas all-time g-local thermality persists, in the above two situations is a clear indication that the two phenomena are fundamentally different and independent from one another.

Lastly, we note that the results of Ref. [50], and therefore of Corollary 1, are proven only for lattices of systems with finite Hilbert-space dimension. In our case, however, the on-site Hilbert-space dimension is infinite. This is not a problem at finite temperatures—the on-site oscillators can be approximated by finite systems by simply cutting off the nearly unpopulated high-energy states. However, the higher the temperatures, the higher the cut-off dimension has to be. And while the increase of the on-site Hilbert-space dimension significantly weakens the bounds established in Ref. [50], interestingly, going to higher temperatures does not affect the precision of all-time g-local thermality in all the systems that we tested.

APPENDIX G: RATE EQUATION IN TTM

According to the TTM [21–27,76], the energy exchange between two coevolving systems is given by the equation

$$\begin{aligned} \frac{dE_A}{dt} &= -(T_A - T_B) k(T_A, T_B), \\ \frac{dE_B}{dt} &= -(T_B - T_A) k(T_A, T_B), \end{aligned} \quad (\text{G1})$$

where the thermal conductance $k(T_A, T_B)$ is positive provided that heat flows from hot to cold.

Introducing the heat capacities for A and B , respectively, as $C_A(T_A)$ and $C_B(T_B)$, we find the time-evolution equation for the temperatures (recalling that the TTM assumes that

A and B are thermal at all times):

$$\begin{aligned} \frac{dT_A}{dt} &= -(T_A - T_B) \frac{k(T_A, T_B)}{C_A(T_A)}, \\ \frac{dT_B}{dt} &= -(T_B - T_A) \frac{k(T_A, T_B)}{C_B(T_B)}. \end{aligned} \quad (\text{G2})$$

Keeping in mind that C_A and C_B are positive quantities, we introduce

$$J(T_A, T_B) := k(T_A, T_B) \left[\frac{1}{C_A(T_A)} + \frac{1}{C_B(T_B)} \right] \geq 0, \quad (\text{G3})$$

and obtain

$$\frac{d(T_A - T_B)}{dt} = -(T_A - T_B) J(T_A, T_B). \quad (\text{G4})$$

This leads us to

$$T_A(t) - T_B(t) = [T_A(0) - T_B(0)] e^{-\int_0^t ds J(T_A(s), T_B(s))}, \quad (\text{G5})$$

which indeed proves that $|T_A(t) - T_B(t)|$ monotonically decreases as the term in the exponent monotonically grows due to J remaining positive at all times.

In fact, the reverse statement is also true: any two monotonically converging differentiable functions $T_A(t)$ and $T_B(t)$ are a solution to a rate equation of the form shown in Eq. (G2). To see this, we note that one can “reverse engineer” Eq. (G5) to obtain the function $J(T_A(t), T_B(t))$, by taking the derivative of $T_A(t) - T_B(t)$. Next, since the heat capacities $C_A(T_A)$ and $C_B(T_B)$ are given, Eq. (G3) can be solved for $k(T_A(t), T_B(t))$. By construction, the solution of Eq. (G2) with the thus-obtained $k(T_A, T_B)$ yields the given functions $T_A(t)$ and $T_B(t)$. Admittedly, this procedure is not useful in practical situations; it is presented here merely to prove the existence of a rate equation.

To summarize, the rate equation in Eq. (G1) and the monotonicity of the convergence of T_A and T_B are equivalent statements. Thus, the second postulate of the TTM can be equivalently rephrased as “the temperatures of the two systems approach each other monotonically in time.”

APPENDIX H: ENERGY OF INTERACTION AT EQUILIBRIUM

Here, we compare the share of H_{int} in the total energy at equilibrium with the precision to which Eq. (16) is satisfied.

The former is given by

$$\mathfrak{R} := \frac{\langle H_{\text{int}} \rangle^{\text{eq}}}{\langle H_A \rangle^{\text{eq}} + \langle H_B \rangle^{\text{eq}}}, \quad (\text{H1})$$

where $\langle H_{\text{int}} \rangle^{\text{eq}} = \text{Tr}[H_{\text{int}} \rho_{AB}^{\text{GGE}}]$, with the other two averages defined analogously. The “precision” of Eq. (16) is

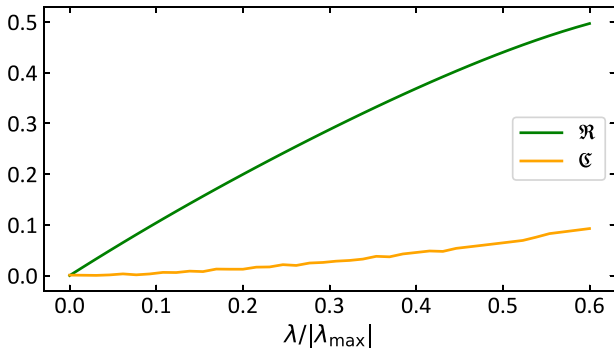


FIG. 16. The role of interaction energy at equilibrium. The plot shows that while, at long times, H_{int} stores a significant amount of energy (green line), its effect on the validity of Eq. (16) remains largely negligible even at strong couplings (orange line). Here, \mathfrak{R} [Eq. (H1)] measures the share of H_{int} in the energy balance at equilibrium and \mathfrak{C} [Eq. (H2)] quantifies the precision to which Eq. (16) is satisfied (with general T_A^{eq} and T_B^{eq}). We see that $\mathfrak{C} \ll 1$ holds as long as the system equilibrates and the choice of $\lambda \leq 0.6 |\lambda_{\text{max}}|$ here ensures that it does. All other parameters are the same as in Fig. 10.

quantified by

$$\mathfrak{C} := 1 - \frac{\langle H_A \rangle_{T_A^{\text{eff,eq}}} + \langle H_B \rangle_{T_B^{\text{eff,eq}}}}{\langle H_A \rangle_{T_A} + \langle H_B \rangle_{T_B}}, \quad (\text{H2})$$

with all the averages defined as in Eq. (16).

We numerically observe that $\mathfrak{C} \ll 1$ even for large values of λ , provided that AB equilibrates at long times. This is contrasted with the fact that $\langle H_{\text{int}} \rangle^{\text{eq}}$ can be significant as compared to $\langle H_A \rangle^{\text{eq}} + \langle H_B \rangle^{\text{eq}}$. These aspects are illustrated in Fig. 16, where we see that $\mathfrak{C} \leq 0.1$ (in fact, remaining much lower than 0.1 up until $\lambda/\lambda_{\text{max}} \approx 0.3$), whereas \mathfrak{R} grows almost linearly with λ , becoming as large as approximately 0.5.

Lastly, note that, when $T_A^{\text{eff,eq}} \neq T_B^{\text{eff,eq}}$, Eq. (16) will not be enough to determine both of these equilibrium temperatures.

-
- [1] J. Gemmer, M. Michel, and G. Mahler, *Quantum Thermodynamics* (Lecture Notes in Physics, Springer-Verlag, Berlin, 2004), Vol. 657.
- [2] A. Polkovnikov, K. Sengupta, A. Silva, and M. Vengalattore, Colloquium: Nonequilibrium dynamics of closed interacting quantum systems, *Rev. Mod. Phys.* **83**, 863 (2011).
- [3] C. Gogolin and J. Eisert, Equilibration, thermalisation, and the emergence of statistical mechanics in closed quantum systems, *Rep. Prog. Phys.* **79**, 056001 (2016).
- [4] T. Mori, T. N. Ikeda, E. Kaminishi, and M. Ueda, Thermalization and prethermalization in isolated quantum systems: A theoretical overview, *J. Phys. B* **51**, 112001 (2018).

- [5] R. Orús, A practical introduction to tensor networks: Matrix product states and projected entangled pair states, *Ann. Phys.* **349**, 117 (2014).
- [6] L. Vidmar and M. Rigol, Generalized Gibbs ensemble in integrable lattice models, *J. Stat. Mech.* **2016**, 064007 (2016).
- [7] A. S. Trushechkin, M. Merkli, J. D. Cresser, and J. Anders, Open quantum system dynamics and the mean force Gibbs state, *AVS Quantum Sci.* **4**, 012301 (2022).
- [8] A. M. Alhambra, Quantum many-body systems in thermal equilibrium, [arXiv:2204.08349](https://arxiv.org/abs/2204.08349) [quant-ph] (2022).
- [9] By qualifying a behavior for a setup as “expected,” we emphasize that it is proven to occur for the setup under certain restrictions and is known to sometimes occur also beyond those restrictions but that exceptions are also known. Such a state of affairs is common in statistical physics.
- [10] G. W. Ford, J. T. Lewis, and R. F. O’Connell, Quantum Langevin equation, *Phys. Rev. A* **37**, 4419 (1988).
- [11] H.-P. Breuer and F. Petruccione, *The Theory of Open Quantum Systems* (Oxford University Press, New York, 2002).
- [12] For a limited class of observables, a form of Markovianity can hold under more general conditions [103].
- [13] J. Berges, S. Borsányi, and C. Wetterich, Prethermalization, *Phys. Rev. Lett.* **93**, 142002 (2004).
- [14] M. Gring, M. Kuhnert, T. Langen, T. Kitagawa, B. Rauer, M. Schreitl, I. Mazets, D. Adu Smith, E. Demler, and J. Schmiedmayer, Relaxation and prethermalization in an isolated quantum system, *Science* **337**, 1318 (2012).
- [15] B. Neyenhuis, J. Zhang, P. W. Hess, J. Smith, A. C. Lee, P. Richerme, Z.-X. Gong, A. V. Gorshkov, and C. Monroe, Observation of prethermalization in long-range interacting spin chains, *Sci. Adv.* **3**, e1700672 (2017).
- [16] Y. Tang, W. Kao, K.-Y. Li, S. Seo, K. Mallayya, M. Rigol, S. Gopalakrishnan, and B. L. Lev, Thermalization near Integrability in a Dipolar Quantum Newton’s Cradle, *Phys. Rev. X* **8**, 021030 (2018).
- [17] L. D. Landau and E. M. Lifshitz, *Statistical Physics, Part I* (Pergamon Press, New York, 1980).
- [18] D. Polder and M. Van Hove, Theory of radiative heat transfer between closely spaced bodies, *Phys. Rev. B* **4**, 3303 (1971).
- [19] D. G. Cahill, W. K. Ford, K. E. Goodson, G. D. Mahan, A. Majumdar, H. J. Maris, R. Merlin, and S. R. Phillpot, Nanoscale thermal transport, *J. Appl. Phys.* **93**, 793 (2003).
- [20] A. I. Volokitin and B. N. J. Persson, Near-field radiative heat transfer and noncontact friction, *Rev. Mod. Phys.* **79**, 1291 (2007).
- [21] S. I. Anisimov, A. M. Bonch-Bruевич, M. A. El’yashevich, Y. A. Imas, N. A. Pavlenko, and G. S. Romanov, Effect of powerful light fluxes on metals, *Sov. Phys.—Tech. Phys.* **11**, 945 (1967).
- [22] S. I. Anisimov, B. L. Kapeliovitch, and T. L. Perel’man, Electron emission from metal surfaces exposed to ultrashort laser pulses, *Sov. Phys. JETP* **39**, 375 (1974).
- [23] D. J. Sanders and D. Walton, Effect of magnon-phonon thermal relaxation on heat transport by magnons, *Phys. Rev. B* **15**, 1489 (1977).

- [24] P. B. Allen, Theory of Thermal Relaxation of Electrons in Metals, *Phys. Rev. Lett.* **59**, 1460 (1987).
- [25] L. Jiang and H.-L. Tsai, Improved two-temperature model and its application in ultrashort laser heating of metal films, *J. Heat Transfer* **127**, 1167 (2005).
- [26] Z. Lin, L. V. Zhigilei, and V. Celli, Electron-phonon coupling and electron heat capacity of metals under conditions of strong electron-phonon nonequilibrium, *Phys. Rev. B* **77**, 075133 (2008).
- [27] W. Wang and D. G. Cahill, Limits to Thermal Transport in Nanoscale Metal Bilayers due to Weak Electron-Phonon Coupling in Au and Cu, *Phys. Rev. Lett.* **109**, 175503 (2012).
- [28] L. Waldecker, R. Bertoni, R. Ernstorfer, and J. Vorberger, Electron-Phonon Coupling and Energy Flow in a Simple Metal beyond the Two-Temperature Approximation, *Phys. Rev. X* **6**, 021003 (2016).
- [29] J. Pudell, A. A. Maznev, M. Herzog, M. Kronseder, C. H. Back, G. Malinowski, A. von Reppert, and M. Bargheer, Layer specific observation of slow thermal equilibration in ultrathin metallic nanostructures by femtosecond x-ray diffraction, *Nat. Commun.* **9**, 3335 (2018).
- [30] M. Herzog, A. von Reppert, J.-E. Pudell, C. Henkel, M. Kronseder, C. H. Back, A. A. Maznev, and M. Bargheer, Phonon-dominated energy transport in purely metallic heterostructures, *Adv. Funct. Mater.* **32**, 2206179 (2022).
- [31] A. Ferraro, A. García-Saez, and A. Acín, Intensive temperature and quantum correlations for refined quantum measurements, *Europhys. Lett.* **98**, 10009 (2012).
- [32] M. Kliesch, C. Gogolin, M. J. Kastoryano, A. Riera, and J. Eisert, Locality of Temperature, *Phys. Rev. X* **4**, 031019 (2014).
- [33] S. Hernández-Santana, A. Riera, K. V. Hovhannisyán, M. Perarnau-Llobet, L. Tagliacozzo, and A. Acín, Locality of temperature in spin chains, *New J. Phys.* **17**, 085007 (2015).
- [34] F. Intravaia, R. O. Behunin, C. Henkel, K. Busch, and D. A. R. Dalvit, Failure of Local Thermal Equilibrium in Quantum Friction, *Phys. Rev. Lett.* **117**, 100402 (2016).
- [35] G. W. Ford, M. Kac, and P. Mazur, Statistical mechanics of assemblies of coupled oscillators, *J. Math. Phys.* **6**, 504 (1965).
- [36] N. D. Mermin and N. W. Ashcroft, *Solid State Physics* (Holt, Rinehart, and Winston, New York, 1976).
- [37] L. Onsager, Theories of concentrated electrolytes, *Chem. Rev.* **13**, 73 (1933).
- [38] J. G. Kirkwood, Statistical mechanics of fluid mixtures, *J. Chem. Phys.* **3**, 300 (1935).
- [39] F. Haake and R. Reibold, Strong damping and low-temperature anomalies for the harmonic oscillator, *Phys. Rev. A* **32**, 2462 (1985).
- [40] U. Seifert, First and Second Law of Thermodynamics at Strong Coupling, *Phys. Rev. Lett.* **116**, 020601 (2016).
- [41] C. Jarzynski, Stochastic and Macroscopic Thermodynamics of Strongly Coupled Systems, *Phys. Rev. X* **7**, 011008 (2017).
- [42] H. J. D. Miller, in *Thermodynamics in the Quantum Regime: Fundamental Aspects and New Directions*, edited by F. Binder, L. A. Correa, C. Gogolin, J. Anders, and G. Adesso (Springer International Publishing, Cham, 2018), p. 531.
- [43] J. D. Cresser and J. Anders, Weak and Ultrastrong Coupling Limits of the Quantum Mean Force Gibbs State, *Phys. Rev. Lett.* **127**, 250601 (2021).
- [44] A. Trushechkin, Quantum master equations and steady states for the ultrastrong-coupling limit and the strong-decoherence limit, *Phys. Rev. A* **106**, 042209 (2022).
- [45] C. L. Latune, Steady state in strong system-bath coupling regime: Reaction coordinate versus perturbative expansion, *Phys. Rev. E* **105**, 024126 (2022).
- [46] M. A. Nielsen and I. L. Chuang, *Quantum Computation and Quantum Information* (Cambridge University Press, Cambridge, United Kingdom, 2010).
- [47] As a guideline, target values $\mathcal{F} \geq 0.99$ for the fidelity ($\mathcal{D} \leq 0.1$) are considered high in current quantum technologies (see, e.g., Refs. [119–121]).
- [48] B. Simon, *The Statistical Mechanics of Lattice Gases* (Princeton University Press, Princeton, New Jersey, 1993), Vol. 1.
- [49] M. P. Müller, E. Adlam, L. Masanes, and N. Wiebe, Thermalization and canonical typicality in translation-invariant quantum lattice systems, *Commun. Math. Phys.* **340**, 499 (2015).
- [50] F. G. S. L. Brandão and M. Cramer, Equivalence of statistical mechanical ensembles for non-critical quantum systems, [arXiv:1502.03263](https://arxiv.org/abs/1502.03263) [quant-ph] (2015).
- [51] H. Tasaki, On the local equivalence between the canonical and the microcanonical ensembles for quantum spin systems, *J. Stat. Phys.* **172**, 905 (2018).
- [52] T. Kuwahara and K. Saito, Gaussian concentration bound and ensemble equivalence in generic quantum many-body systems including long-range interactions, *Ann. Phys.* **421**, 168278 (2020).
- [53] S. Goldstein, J. L. Lebowitz, R. Tumulka, and N. Zanghi, Canonical Typicality, *Phys. Rev. Lett.* **96**, 050403 (2006).
- [54] S. Popescu, A. J. Short, and A. Winter, Entanglement and the foundations of statistical mechanics, *Nat. Phys.* **2**, 754 (2006).
- [55] T. Farrelly, F. G. S. L. Brandão, and M. Cramer, Thermalization and Return to Equilibrium on Finite Quantum Lattice Systems, *Phys. Rev. Lett.* **118**, 140601 (2017).
- [56] G. Adesso and F. Illuminati, Entanglement in continuous-variable systems: Recent advances and current perspectives, *J. Phys. A* **40**, 7821 (2007).
- [57] J. Anders, Thermal state entanglement in harmonic lattices, *Phys. Rev. A* **77**, 062102 (2008).
- [58] C. Weedbrook, S. Pirandola, R. García-Patrón, N. J. Cerf, T. C. Ralph, J. H. Shapiro, and S. Lloyd, Gaussian quantum information, *Rev. Mod. Phys.* **84**, 621 (2012).
- [59] M. Tegmark and L. Yeh, Steady states of harmonic oscillator chains and shortcomings of harmonic heat baths, *Physica A* **202**, 342 (1994).
- [60] Y. Subaşı, C. H. Fleming, J. M. Taylor, and B.-L. Hu, Equilibrium states of open quantum systems in the strong coupling regime, *Phys. Rev. E* **86**, 061132 (2012).
- [61] For fixed ω_X 's and α , the requirement that H_{tot} must be bounded from below sets an upper bound on $|g_X|$ and $|\lambda|$.
- [62] Note that the stabilization of $\mathcal{F}_X^{\text{max}}$ does not imply that the states $\rho_X(t)$ themselves stabilize—it is just their distance from the set of Gibbs states that stabilizes.

- [63] N. Linden, S. Popescu, A. J. Short, and A. Winter, Quantum mechanical evolution towards thermal equilibrium, *Phys. Rev. E* **79**, 061103 (2009).
- [64] M. Cramer and J. Eisert, A quantum central limit theorem for non-equilibrium systems: Exact local relaxation of correlated states, *New J. Phys.* **12**, 055020 (2010).
- [65] T. Kinoshita, T. Wenger, and D. S. Weiss, A quantum Newton's cradle, *Nature* **440**, 900 (2006).
- [66] M. Rigol, V. Dunjko, V. Yurovsky, and M. Olshanii, Relaxation in a Completely Integrable Many-Body Quantum System: An *Ab Initio* Study of the Dynamics of the Highly Excited States of 1D Lattice Hard-Core Bosons, *Phys. Rev. Lett.* **98**, 050405 (2007).
- [67] M. Rigol, V. Dunjko, and M. Olshanii, Thermalization and its mechanism for generic isolated quantum systems, *Nature* **452**, 854 (2008).
- [68] T. Barthel and U. Schollwöck, Dephasing and the Steady State in Quantum Many-Particle Systems, *Phys. Rev. Lett.* **100**, 100601 (2008).
- [69] M. Fagotti, On conservation laws, relaxation and pre-relaxation after a quantum quench, *J. Stat. Mech.* **2014**, P03016 (2014).
- [70] T. Langen, S. Erne, R. Geiger, B. Rauer, T. Schweigler, M. Kuhnert, W. Rohringer, I. E. Mazets, T. Gasenzer, and J. Schmiedmayer, Experimental observation of a generalized Gibbs ensemble, *Science* **348**, 207 (2015).
- [71] F. H. L. Essler and M. Fagotti, Quench dynamics and relaxation in isolated integrable quantum spin chains, *J. Stat. Mech.* **2016**, 064002 (2016).
- [72] F. Kranzl, A. Lasek, M. K. Joshi, A. Kalev, R. Blatt, C. F. Roos, and N. Yunger Halpern, Experimental Observation of Thermalization with Noncommuting Charges, *PRX Quantum* **4**, 020318 (2023).
- [73] C. Murthy and M. Srednicki, Relaxation to Gaussian and generalized Gibbs states in systems of particles with quadratic Hamiltonians, *Phys. Rev. E* **100**, 012146 (2019).
- [74] M. Gluza, J. Eisert, and T. Farrelly, Equilibration towards generalized Gibbs ensembles in non-interacting theories, *SciPost Phys.* **7**, 038 (2019).
- [75] E. Carpena, Ultrafast laser irradiation of metals: Beyond the two-temperature model, *Phys. Rev. B* **74**, 024301 (2006).
- [76] B. Liao, J. Zhou, and G. Chen, Generalized Two-Temperature Model for Coupled Phonon-Magnon Diffusion, *Phys. Rev. Lett.* **113**, 025902 (2014).
- [77] A. von Reppert, J. Pudell, A. Koc, M. Reinhardt, W. Leitenberger, K. Dumesnil, F. Zamponi, and M. Bargheer, Persistent nonequilibrium dynamics of the thermal energies in the spin and phonon systems of an antiferromagnet, *Struct. Dyn.* **3**, 054302 (2016).
- [78] J. Byskov-Nielsen, J.-M. Savolainen, M. S. Christensen, and P. Balling, Ultra-short pulse laser ablation of copper, silver and tungsten: Experimental data and two-temperature model simulations, *Appl. Phys. A* **103**, 447 (2011).
- [79] E. Beaurepaire, J.-C. Merle, A. Daunois, and J.-Y. Bigot, Ultrafast Spin Dynamics in Ferromagnetic Nickel, *Phys. Rev. Lett.* **76**, 4250 (1996).
- [80] G. Zhang, W. Hübner, E. Beaurepaire, and J.-Y. Bigot, in *Spin Dynamics in Confined Magnetic Structures I*, edited by B. Hillebrands and K. Ounadjela (Springer-Verlag, Berlin, 2002), p. 245.
- [81] N. Kazantseva, U. Nowak, R. W. Chantrell, J. Hohlfeld, and A. Rebei, Slow recovery of the magnetisation after a sub-picosecond heat pulse, *Europhys. Lett.* **81**, 27004 (2007).
- [82] P. Maldonado, K. Carva, M. Flammer, and P. M. Oppeneer, Theory of out-of-equilibrium ultrafast relaxation dynamics in metals, *Phys. Rev. B* **96**, 174439 (2017).
- [83] J.-E. Pudell, M. Mattern, M. Hehn, G. Malinowski, M. Herzog, and M. Bargheer, Heat transport without heating?—An ultrafast x-ray perspective into a metal heterostructure, *Adv. Funct. Mater.* **30**, 2004555 (2020).
- [84] R. Schmidt, S. Maniscalco, and T. Ala-Nissila, Heat flux and information backflow in cold environments, *Phys. Rev. A* **94**, 010101(R) (2016).
- [85] V. Bendkowsky, B. Butscher, J. Nipper, J. P. Shaffer, R. Löw, and T. Pfau, Observation of ultralong-range Rydberg molecules, *Nature* **458**, 1005 (2009).
- [86] J. W. Britton, B. C. Sawyer, A. C. Keith, C.-C. J. Wang, J. K. Freericks, H. Uys, M. J. Biercuk, and J. J. Bollinger, Engineered two-dimensional Ising interactions in a trapped-ion quantum simulator with hundreds of spins, *Nature* **484**, 489 (2012).
- [87] C. Gross and I. Bloch, Quantum simulations with ultracold atoms in optical lattices, *Science* **357**, 995 (2017).
- [88] H. Bernien, S. Schwartz, A. Keesling, H. Levine, A. Omran, H. Pichler, S. Choi, A. S. Zibrov, M. Endres, M. Greiner, V. Vuletic, and M. D. Lukin, Probing many-body dynamics on a 51-atom quantum simulator, *Nature* **551**, 579 (2017).
- [89] A. De Pasquale and T. M. Stace, in *Thermodynamics in the Quantum Regime: Fundamental Aspects and New Directions*, edited by F. Binder, L. A. Correa, C. Gogolin, J. Anders, and G. Adesso (Springer International Publishing, Cham, 2018), p. 503.
- [90] M. Mehboudi, A. Sanpera, and L. A. Correa, Thermometry in the quantum regime: Recent theoretical progress, *J. Phys. A* **52**, 303001 (2019).
- [91] A. De Pasquale, D. Rossini, R. Fazio, and V. Giovannetti, Local quantum thermal susceptibility, *Nat. Commun.* **7**, 12782 (2016).
- [92] S. Campbell, M. Mehboudi, G. De Chiara, and M. Paternostro, Global and local thermometry schemes in coupled quantum systems, *New J. Phys.* **19**, 103003 (2017).
- [93] K. V. Hovhannisyann and L. A. Correa, Measuring the temperature of cold many-body quantum systems, *Phys. Rev. B* **98**, 045101 (2018).
- [94] H. J. D. Miller and J. Anders, Energy-temperature uncertainty relation in quantum thermodynamics, *Nat. Commun.* **9**, 2203 (2018).
- [95] M. Perarnau-Llobet, H. Wilming, A. Riera, R. Gallego, and J. Eisert, Strong Coupling Corrections in Quantum Thermodynamics, *Phys. Rev. Lett.* **120**, 120602 (2018).
- [96] K. V. Hovhannisyann, F. Barra, and A. Imparato, Charging assisted by thermalization, *Phys. Rev. Res.* **2**, 033413 (2020).
- [97] C. Henkel, Heat transfer and entanglement–non-equilibrium correlation spectra of two quantum oscillators, *Ann. Phys.* **533**, 2100089 (2021).

- [98] N. Anto-Sztrikacs, F. Ivander, and D. Segal, Quantum thermal transport beyond second order with the reaction coordinate mapping, *J. Chem. Phys.* **156**, 214107 (2022).
- [99] O. A. Castro-Alvaredo, B. Doyon, and T. Yoshimura, Emergent Hydrodynamics in Integrable Quantum Systems out of Equilibrium, *Phys. Rev. X* **6**, 041065 (2016).
- [100] V. B. Bulchandani, R. Vasseur, C. Karrasch, and J. E. Moore, Solvable Hydrodynamics of Quantum Integrable Systems, *Phys. Rev. Lett.* **119**, 220604 (2017).
- [101] G. Manzano, J. M. R. Parrondo, and G. T. Landi, Non-Abelian Quantum Transport and Thermosqueezing Effects, *PRX Quantum* **3**, 010304 (2022).
- [102] S. Majidy, A. Lasek, D. A. Huse, and N. Yunger Halpern, Non-Abelian symmetry can increase entanglement entropy, *Phys. Rev. B* **107**, 045102 (2023).
- [103] P. Strasberg, A. Winter, J. Gemmer, and J. Wang, Classicality, Markovianity and local detailed balance from pure-state dynamics, *Phys. Rev. A* **108**, 012225 (2023).
- [104] H. Scutaru, Fidelity for displaced squeezed thermal states and the oscillator semigroup, *J. Phys. A* **31**, 3659 (1998).
- [105] P. Marian and T. A. Marian, Uhlmann fidelity between two-mode Gaussian states, *Phys. Rev. A* **86**, 022340 (2012).
- [106] L. Banchi, S. L. Braunstein, and S. Pirandola, Quantum Fidelity for Arbitrary Gaussian States, *Phys. Rev. Lett.* **115**, 260501 (2015).
- [107] R. H. Swendsen, Continuity of the entropy of macroscopic quantum systems, *Phys. Rev. E* **92**, 052110 (2015).
- [108] U. Seifert, Entropy and the second law for driven, or quenched, thermally isolated systems, *Physica A* **552**, 121822 (2020).
- [109] P. Strasberg and A. Winter, First and Second Law of Quantum Thermodynamics: A Consistent Derivation Based on a Microscopic Definition of Entropy, *PRX Quantum* **2**, 030202 (2021).
- [110] J. Williamson, On the algebraic problem concerning the normal forms of linear dynamical systems, *Am. J. Math.* **58**, 141 (1936).
- [111] V. I. Arnold, *Mathematical Methods of Classical Mechanics* (Springer, New York, 1989), 2nd ed.
- [112] H. Heffner and W. H. Louisell, Transformation having applications in quantum mechanics, *J. Math. Phys.* **6**, 474 (1965).
- [113] E. G. Brown, E. Martín-Martínez, N. C. Menicucci, and R. B. Mann, Detectors for probing relativistic quantum physics beyond perturbation theory, *Phys. Rev. D* **87**, 084062 (2013).
- [114] N. Shiraishi and K. Matsumoto, Undecidability in quantum thermalization, *Nat. Commun.* **12**, 5084 (2021).
- [115] C. A. Fuchs and J. van de Graaf, Cryptographic distinguishability measures for quantum-mechanical states, *IEEE Trans. Inf. Theory* **45**, 1216 (1999).
- [116] M. Cramer and J. Eisert, Correlations, spectral gap and entanglement in harmonic quantum systems on generic lattices, *New J. Phys.* **8**, 71 (2006).
- [117] J. Barré, D. Mukamel, and S. Ruffo, Inequivalence of Ensembles in a System with Long-Range Interactions, *Phys. Rev. Lett.* **87**, 030601 (2001).
- [118] A. Campa, T. Dauxois, and S. Ruffo, Statistical mechanics and dynamics of solvable models with long-range interactions, *Phys. Rep.* **480**, 57 (2009).
- [119] C. E. Bradley, J. Randall, M. H. Abobeih, R. C. Berrevoets, M. J. Degen, M. A. Bakker, M. Markham, D. J. Twitchen, and T. H. Taminiau, A Ten-Qubit Solid-State Spin Register with Quantum Memory up to One Minute, *Phys. Rev. X* **9**, 031045 (2019).
- [120] Y. Zhou, E. M. Stoudenmire, and X. Waintal, What Limits the Simulation of Quantum Computers?, *Phys. Rev. X* **10**, 041038 (2020).
- [121] M. S. Rudolph, N. B. Toussaint, A. Katarbarwa, S. Johri, B. Peropadre, and A. Perdomo-Ortiz, Generation of High-Resolution Handwritten Digits with an Ion-Trap Quantum Computer, *Phys. Rev. X* **12**, 031010 (2022).